SPECIAL ISSUE ARTICLE

Dynamics and quantum correlations in two independently driven Rydberg atoms with distinct laser fields

IOP Publishing Journal of Physics B: Atomic, Molecular and Optical Physics
J. Phys. B: At. Mol. Opt. Phys. **52** (2019) 184001 (15pp) https://doi.org/10.1088/1361-6455/ab32a2

Dynamics and quantum correlations in two independently driven Rydberg atoms with distinct laser fields

Vineesha Srivastava[1,2,3], **Ankita Niranjan**[1] and **Rejish Nath**[1]

[1] Indian Institute of Science Education and Research, Pune 411 008, India
[2] Indian Institute of Technology (BHU), Varanasi 221 005, India

E-mail: vineeshavineet@gmail.com

Received 2 May 2019, revised 5 July 2019
Accepted for publication 16 July 2019
Published 22 August 2019

Abstract

We study the population dynamics in a two-atom setup in which each atom is driven independently by different light fields, but coupling the same Rydberg state. In particular, we look at how an offset in the Rabi frequencies between two atoms affects the dynamics. We find novel features such as amplifying the Rabi frequency of one atom, together with strong Rydberg-Rydberg interactions freezes the dynamics in the second atom. We analyze this Rydberg-biased freezing phenomenon in detail, with effective Hamiltonians obtained for various limits of the system parameters. In the absence of Rabi-offset, the doubly excited state population exhibits a Lorentzian profile as a function of interaction, whereas for very small offsets it shows splitting and thus peaks. Using an effective Hamiltonian, as well as the perturbation theory in the weak interaction limit, we show that the peak arises from a competition between Rabi-offset and Rydberg-Rydberg interactions when both are sufficiently small, together with the Rydberg blockade at large interactions. The effective Hamiltonians provide us with analytical results for long time dynamics, which are in an excellent agreement with exact numerical solutions. Also, we analyze the growth and the dynamics of quantum correlations such as entanglement entropy/quantum discord for the coherent dynamics. Finally, we extend our studies to the dissipative case in which the spontaneous emission from the Rydberg state is taken into account and in particular, we look at how the Rabi-offset modifies the purity and quantum discord in the steady states. We conclude that the local manipulation of an atom by introducing a Rabi-offset can be a useful tool to control the quantum correlations and in general, the quantum states of the composite two-qubit systems.

Keywords: Rydberg atoms, coherent quantum control, Rydberg blockade

(Some figures may appear in colour only in the online journal)

1. Introduction

Rydberg excited atoms have emerged as a great platform to test and study various quantum phenomena [1–4], due to the multifaceted nature in engineering their properties using external fields. In particular, the strong Rydberg–Rydberg interactions [5] lead to a well-known phenomenon called the Rydberg or dipole blockade [6–8] and is a crucial mechanism for applications from quantum many-body physics [9–17] to quantum information protocols [1, 18–21].

A typical Rydberg setup has been modeled as a gas of interacting two-level atoms (qubits), with interactions of either dipolar or van der Waals type. The minimal setup constitutes of either two atoms or two excitations and has been a usual scenario in many of the Rydberg-based experimental studies [5, 7, 8, 19, 20, 22–30]. On an equivalent note, the atom-based technologies have progressed in such a way that it is possible to probe and manipulate at a single particle level [17, 31, 32]. Recently, involving Rydberg excitations, single atom addressing has been used to quantify the imperfections in Rabi oscillations [33], proposed to engineer phonon modes in ion crystals [34, 35], to achieve controlled local operations to manipulate two atom

[3] Author to whom any correspondence should be addressed.

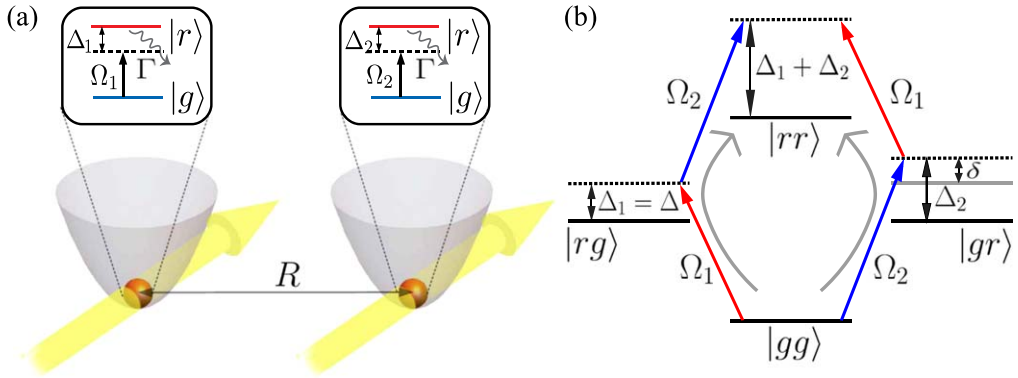

Figure 1. (a) Schematic picture of two atoms trapped using microtraps with a separation of R. Each of the atoms is assumed to be driven independently by different laser fields, but they couple the ground state $|g\rangle$ to the same Rydberg state $|r\rangle$. Γ is the decay rate from the Rydberg state $|r\rangle$. (b) shows the level scheme for two atoms and the corresponding laser parameters associated with each state including the Rabi couplings. The two primary trajectories by which the state $|rr\rangle$ is populated from $|gg\rangle$, via $|gr\rangle$ and $|rg\rangle$ are shown by curved arrows.

quantum states [24], controlling resonant dipole–dipole interaction between Rydberg atoms [3], as well as freezing spin excitation dynamics [27] and controlled quantum gates [30, 36].

On the other side, to characterize quantum correlations in composite systems is a nontrivial and important task for developing scalable quantum technologies. In particular, entanglement entropy and quantum discord have gained a vital importance because of their applications in condensed matter physics, especially in characterizing various quantum phases [37–44], including topologically ordered ones [42, 45–47] and spin liquids [48, 49]. While entanglement entropy measures the entanglement between two subsystems [50, 51] in pure states, discord is treated as a more general non-classical correlation, may possess a nonzero value even for separable mixed states [52, 53] and is highly relevant for deterministic quantum computation with a single qubit [44, 54–56]. Associated to entanglement entropy in pure states, an alternate measure for entanglement in mixed states is the entanglement of formation [50]. So far, using ultracold atomic setups, only the dynamics of entanglement (Rényi) entropy have been measured in quantum quench experiments [57, 58].

In this paper, motivated by the above developments on single particle control and manipulation, we study a minimal setup of two two-level Rydberg atoms driven continuously and independently by two distinct laser fields. In particular, we look at the effect of an offset in Rabi frequencies between the fields on the population dynamics, in the presence of Rydberg–Rydberg interactions. Interestingly, the population dynamics reveal qualitatively novel features. An interesting scenario emerges when amplifying the Rabi coupling in one atom freezes the dynamics in the second atom, in the presence of strong atom–atom interactions. This phenomenon we term as *Rydberg-biased freezing*, and is well captured by the effective Hamiltonians at different limits of system parameters. Without the Rabi-offset, the time-averaged doubly excited state population exhibits a Lorentzian profile as a function of interaction strength. Whereas for small offset, the Lorentzian profile gets deformed, showing a non-monotonous behaviour with peaks at small interaction strengths. Anew, obtaining an effective Hamiltonian, as well as using the second order perturbation theory, we show that the peak arises from a competition between the Rabi-offset and the Rydberg–Rydberg interaction when both are sufficiently small, together with Rydberg blockade at large interactions. The striking quality of the effective Hamiltonians obtained is that we can attain analytical solutions for long-time dynamics for the various limits. Further, we analyze the growth and temporal evolution of quantum correlations such as the entanglement entropy or the quantum discord for the coherent dynamics. While entanglement entropy serves as a good measure for quantum correlations only in pure states, the quantum discord is used for both pure and mixed states. The correlation dynamics also reveals the competition between the inter-atomic interactions and Rabi-offset when both are sufficiently small. We extend our studies to the dissipative case in which the spontaneous emission from the Rydberg state is taken into account and in particular, we look at the effect of Rabi-offset on the purity and quantum discord in the steady states [59, 60]. Finally, we demonstrate and conclude that the Rabi-offset can constitute an easy tool to control quantum correlations between the composite two-qubit systems.

The paper is structured as follows. In section 2 we discuss the schematic setup, the model Hamiltonian, the master equation and define the quantum correlations that we analyze. In section 3 we study the coherent dynamics of the system as a function of Rabi-offset and interaction strength. In section 4 we obtain effective Hamiltonians describing the long-time dynamics in various limits of the system parameters. In section 5 we study the dynamics of quantum correlations such as entanglement entropy/quantum discord for the coherent dynamics discussed in section 3. Finally, in section 6 we consider the spontaneous emission from the Rydberg state and look at the dynamics and steady-state quantum correlations. In the appendix, we provide details on the perturbation theory calculations in the weak-interaction limit as well as the analytical results for the steady state density matrices and purity for the system and subsystems.

2. Setup, model and quantum correlations

We consider two two-level atoms or qubits, each of them being strongly confined in two independent micro traps (see

figure 1(a)), and are driven by distinct laser fields with Rabi frequencies Ω_i and detunings Δ_i, coupling the electronic ground state $|g\rangle$ to a Rydberg state $|r\rangle$. Let $V_0 = C_6/R^6$ provides us with the strength of the van der Waals interaction between the two Rydberg excited atoms. In the frozen gas limit [61, 62], ignoring the motional dynamics of the atoms, the internal state dynamics of the setup is governed by the Hamiltonian ($\hbar = 1$):

$$\hat{H} = -\sum_{i=1}^{2} \Delta_i \hat{\sigma}_{rr}^i + \sum_{i=1}^{2} \frac{\Omega_i}{2} \hat{\sigma}_x^i + V_0 \hat{\sigma}_{rr}^1 \hat{\sigma}_{rr}^2, \tag{1}$$

where $\hat{\sigma}_{ab} = |a\rangle\langle b|$ with $a, b \in \{r, g\}$, $\hat{\sigma}_x = \hat{\sigma}_{rg} + \hat{\sigma}_{gr}$. Introducing $\Delta_1 = \Delta$, $\Delta_2 = \Delta + \delta$, $\Omega_1 = \Omega$ and $\Omega_2 = \Omega + \omega$ with $\omega > 0$, we rewrite the Hamiltonian in equation (1) as,

$$\hat{H} = -\Delta \sum_{i=1}^{2} \hat{\sigma}_{rr}^i + \frac{\Omega}{2} \sum_{i=1}^{2} \hat{\sigma}_x^i + V_0 \hat{\sigma}_{rr}^1 \hat{\sigma}_{rr}^2 - \delta \hat{\sigma}_{rr}^2 + \frac{\omega}{2} \hat{\sigma}_x^2. \tag{2}$$

In the absence of Rabi couplings ($\Omega = \omega = 0$), the eigenstates of the Hamiltonian in equation (2) are $|gg\rangle$, $|rg\rangle$, $|gr\rangle$ and $|rr\rangle$ with eigenvalues $E_{gg} = 0$, $E_{rg} = -\Delta$, $E_{gr} = -\Delta - \delta$ and $E_{rr} = -2\Delta - \delta + V_0$. The coherent dynamics of the system is obtained by numerically solving the Schrödinger equation: $i\partial/\partial t|\psi(t)\rangle = \hat{H}|\psi(t)\rangle$ and we use the two-atom basis $\{|gg\rangle, |gr\rangle, |rg\rangle, |rr\rangle\}$. Throughout we take $|\psi(t = 0)\rangle = |gg\rangle$ and assume both the fields are at resonance ($\delta = \Delta = 0$) with $|g\rangle - |r\rangle$ transition and we focus on how the Rabi-offset ω affects the population dynamics. With the above assumptions, the Hamiltonian reduces to

$$\hat{H} = \frac{\Omega}{2} \sum_{i=1}^{2} \hat{\sigma}_x^i + \frac{\omega}{2} \hat{\sigma}_x^2 + V_0 \hat{\sigma}_{rr}^1 \hat{\sigma}_{rr}^2. \tag{3}$$

The level scheme of our two-atom setup with laser parameters is shown in figure 1(b) and the two primary trajectories by which the state $|rr\rangle$ is populated from $|gg\rangle$, via $|gr\rangle$ and $|rg\rangle$ are shown by curved arrows. When ω vanishes, the system is identical to the scenario in which both the atoms are driven by a global field. In that case, for sufficiently large V_0 ($>\Omega$) starting from $|gg\rangle$, the system undergoes coherent Rabi oscillations between $|gg\rangle$ and $|+\rangle = (|gr\rangle + |rg\rangle)/\sqrt{2}$ with an enhanced Rabi frequency of $\sqrt{2}\,\Omega$. These dynamics are attributed to the Rydberg blockade. A non zero ω breaks the symmetry between the two atoms and hence, the state $|+\rangle$ lost its significance in the dynamics.

Apart from the state dynamics, we also look at how the quantum correlations develop and evolve in our setup in particular, the entanglement entropy or the quantum discord. Since the initial state $|gg\rangle$ is not an eigenstate of the Hamiltonian given in equation (3), our scenario is identical to that of a quantum quench problem in which the Rabi frequencies are instantaneously quenched from zero to a finite value at $t = 0$. Let us label the first atom as subsystem A and the strongly driven second atom as subsystem B. The entanglement entropy of the subsystems are $\mathcal{S}_A = -\mathrm{Tr}(\hat{\rho}_A \log_2 \hat{\rho}_A)$ and $\mathcal{S}_B = -\mathrm{Tr}(\hat{\rho}_B \log_2 \hat{\rho}_B)$ where $\hat{\rho}_A$ ($\hat{\rho}_B$) is the reduced density matrix for A (B), which is obtained by the partial trace of the total density matrix, $\hat{\rho} = |\psi(t)\rangle\langle\psi(t)|$. The partial trace over ρ leaves the subsystems A and B in a classical mixture of pure

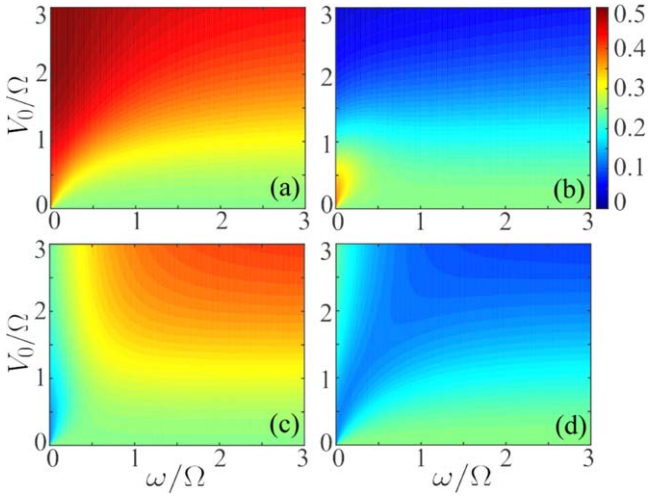

Figure 2. Density plot for time average populations: (a) $\bar{P}_{gg}$, (b) $\bar{P}_{rr}$, (c) $\bar{P}_{gr}$ and (d) $\bar{P}_{rg}$ as a function of V_0/Ω and ω/Ω for $\Delta = \delta = 0$ and $|\psi(t = 0)\rangle = |gg\rangle$ at $\Omega\tau = 5000$. For large values of V_0/Ω and ω/Ω both $\bar{P}_{rr}$ and $\bar{P}_{rg}$ are negligible, leading to the phenomenon of Rydberg-biased freezing. Also (b) reveals us that the blockade condition is weakly affected by the Rabi-offset ω.

quantum states. In terms of the eigenvalues (λ_i) of $\hat{\rho}_A$, we have $\mathcal{S}_A = -\sum_{i=1}^{2} \lambda_i \log_2 \lambda_i$, and for a pure state $\mathcal{S}_A = \mathcal{S}_B$.

To define the quantum discord, we briefly sketch the mutual information in the classical information theory. The classical mutual information between two subsystems A and B is defined as $\mathcal{I} = H_A + H_B - H_{AB}$ where H_A (H_B) is the Shannon entropy of the subsystem A (B), and H_{AB} is the joint entropy of A and B. An equivalent expression for mutual information is $\mathcal{J} = H_B - H_{B|A}$, where $H_{B|A}$ is the conditional entropy, the information needed to describe B when A is known. Though, in the classical theory $\mathcal{I} = \mathcal{J}$, in the quantum version, in which the Shannon entropy is replaced by the von Neumann entropy, a discrepancy between $\mathcal{I}$ and $\mathcal{J}$ exists, which is quantified by the quantum discord.

In the quantum theory, we have $\mathcal{I} = \mathcal{S}_A + \mathcal{S}_B - \mathcal{S}_{AB}$ and $\mathcal{J}(B : A) = \mathcal{S}_B - \mathcal{S}_{B|A}$, where $\mathcal{S}_{AB} = -\mathrm{Tr}(\hat{\rho} \log_2 \hat{\rho})$ is the von Neumann entropy for the state $\hat{\rho}$, and $\mathcal{S}_{AB} = 0$ for a pure state. Given a complete set of von Neuman projective measurements $\{\hat{\Pi}_A^i\}$ on the subsystem A with probabilities $\{p^i\}$, the conditional entropy of the subsystem B is $\mathcal{S}_{B|A} = \sum_i p^i \mathcal{S}_{B|i}$, where $\mathcal{S}_{B|i}$ is the von Neumann entropy for the reduced density operator $\hat{\rho}_B^i = \mathrm{Tr}_A[(\hat{\Pi}_A^i \otimes \mathbb{I}_B)\hat{\rho}_{AB}(\hat{\Pi}_A^i \otimes \mathbb{I}_B)^\dagger]/p^i$ with $p^i = \mathrm{Tr}_{AB}[(\hat{\Pi}_A^i \otimes \mathbb{I}_B)\hat{\rho}_{AB}(\hat{\Pi}_A^i \otimes \mathbb{I}_B)^\dagger]$ and $\mathbb{I}_B$ is the identity operator. It has been shown that the total classical correlation can be obtained as $\tilde{\mathcal{J}}(B\colon A) = \max_{\{\hat{\Pi}_A^i\}}[\mathcal{S}_B - \sum_i p^i \mathcal{S}_{B|i}]$ [52]. The maximization ($\max_{\{\hat{\Pi}_A^i\}}$) is carried across all the possible orthonormal measurement bases $\{\hat{\Pi}_A^i\}$ of subsystem A. Similarly one can obtain $\tilde{\mathcal{J}}(A\colon B)$ where the measurements are being carried out on subsystem B. Finally, the quantum discord is defined on both ways by swapping A and B as,

$$\mathcal{D}(A : B) = \mathcal{I} - \tilde{\mathcal{J}}(A\colon B), \tag{4}$$

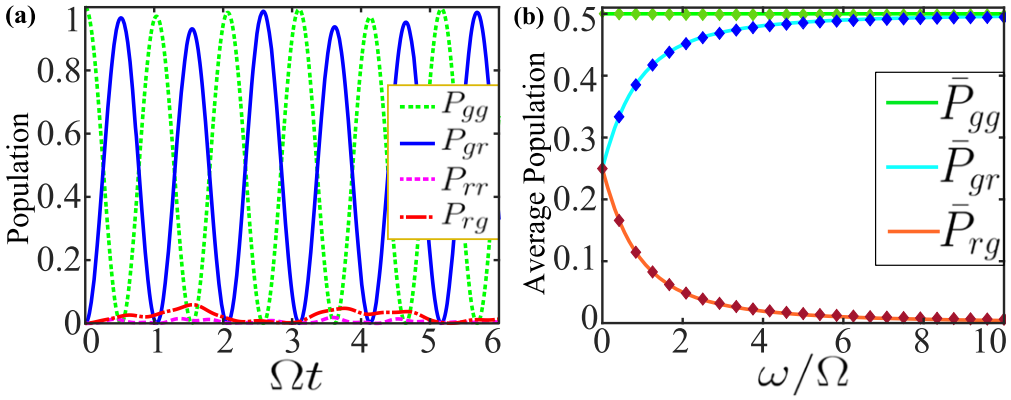

Figure 3. (a) The population dynamics at $V_0/\Omega = 10$ and $\omega/\Omega = 5$. (b) The time average populations as a function of ω/Ω for $V_0 = 25\Omega$, $\delta = 0$ and $\Omega\tau = 5000$. Since $V_0 \gg \Omega$, the numerical results (solid points) are in excellent agreement with the analytic results (solid lines) given in equations (10)–(12).

and

$$\mathcal{D}(B : A) = \mathcal{I} - \tilde{\mathcal{J}}(B{:}\, A). \tag{5}$$

Note that the quantum conditional entropy depends on the choice of the observables being measured on the other subsystem, and this results in a discrepancy between $\mathcal{I}$ and $\mathcal{J}(B : A)$ or $\mathcal{J}(A : B)$, which is quantified as the quantum discord. For a bipartite pure state $|\psi(t)\rangle$ the quantum discord coincides with the entanglement entropy, i.e., $\mathcal{D}(A : B) = \mathcal{D}(B : A) = \mathcal{S}_A = \mathcal{S}_B$ [63].

Once the spontaneous emission from the Rydberg state is taken into account, the dissipative dynamics and the steady state correlations are analyzed using the master equation for the two-particle density matrix $\hat{\rho}$,

$$\partial_t\hat{\rho} = -i[\hat{H},\, \hat{\rho}] + \mathcal{L}[\hat{\rho}], \tag{6}$$

with the Lindblad operator given by

$$\mathcal{L}[\hat{\rho}] = \sum_{i=1}^{2} \hat{C}_i\hat{\rho}\hat{C}_i^{\dagger} - \frac{1}{2}\sum_i(\hat{C}_i^{\dagger}\hat{C}_i\hat{\rho} + \hat{\rho}\hat{C}_i^{\dagger}\hat{C}_i) \tag{7}$$

where the operator, $\hat{C}_i = \sqrt{\Gamma}\,\hat{\sigma}_{ge}^{i}$ with Γ as the spontaneous decay rate of the Rydberg state $|r\rangle$. At the steady state, $\partial_t\hat{\rho} = 0$ and the dissipative mechanism drives the system eventually into a mixed state even though the system is initially prepared in a pure state. Note that, for a mixed state, the discord is no longer the same as the entanglement entropy and, infact, $\mathcal{S}_{A,B}$ has been ruled out from being a good measure of quantum correlations or entanglement since it fails to distinguish between classical and quantum correlations [50, 64, 65], whereas the quantum discord remains a good measure. For a mixed state in general, $\mathcal{D}(A{:}\, B) \neq \mathcal{D}(B : A)$ since the conditional entropy is not symmetric for all states [38]. The exception is, i.e. $\mathcal{D}(A : B) = \mathcal{D}(B : A)$ when the states are symmetric under the exchange of A and B.

3. State population dynamics

Here, we analyze the effect of Rabi-offset ω on the Rydberg excitation dynamics, in particular, how it affects the Rydberg blockade. We look at the time averaged populations (see figures 2 and 3): $\bar{P}_{\alpha\beta} = 1/\tau\int_0^{\tau} P_{\alpha\beta}(t)dt$ with $\alpha, \beta \in \{r, g\}$ of the states $\{|\alpha\beta\rangle\}$, as a function of ω and V_0. For $\omega = 0$ and sufficiently large V_0/Ω, the interaction induced level shift in $|rr\rangle$ state results in the well-known Rydberg blockade with average populations approaching $\bar{P}_{gg} \to 0.5$, $\bar{P}_{rr} \to 0$, $\bar{P}_{+} \to 0.5$, where $P_{+} = P_{rg} + P_{gr}$. For $\omega \ll \Omega$, we have $\bar{P}_{gr} \approx \bar{P}_{rg}$ independently of V_0. When ω is significantly large, the results shown in figure 2 reveal interesting features. The first thing to notice from figure 2(b) is that the blockade condition is merely affected by ω for sufficiently large ω. This is understood as follows: as ω becomes large, the second atom is driven strongly compared to the first one, and that results in the augmentation of P_{gr} at the cost of P_{rg}. Hence, to attain blockade the Rydberg–Rydberg interactions just have to dominate the Rabi coupling of the weakly driven atom, i.e., $V_0 > \Omega$, leaving the blockade condition almost independent of ω, which becomes more apparent in section 4. It also implies that the blockade dynamics do not necessarily always result in the generation of the symmetric entangled state $|+\rangle$ as in the case for $\omega = 0$. Summing up, we have an interesting scenario: for sufficiently large ω/Ω and V_0/Ω, the dynamics of the first atom nearly freezes and the system exhibits coherent Rabi oscillations between $|gg\rangle$ and $|gr\rangle$ with $P_{rr} \approx 0$ and $P_{rg} \approx 0$ as shown in figures 3. Note that the freezing of the first atom emerges as a combined effect of both the Rydberg blockade from large interactions and the strong driving in the second atom, and we term this as *Rydberg-biased freezing*.

To gain more insights into the population dynamics, in figure 4 we show explicitly the average populations as a function of V_0/Ω for different values of ω/Ω. When $V_0 = 0$, the two atom states are simply the product of single-atom states and we have $P_{gg}(t) = \cos^2\frac{\Omega t}{2}\cos^2\frac{(\Omega+\omega)t}{2}$, $P_{gr}(t) = \cos^2\frac{\Omega t}{2}\sin^2\frac{(\Omega+\omega)t}{2}$, $P_{rg}(t) = \sin^2\frac{\Omega t}{2}\cos^2\frac{(\Omega+\omega)t}{2}$ and $P_{rr}(t) = \sin^2\frac{\Omega t}{2}\sin^2\frac{(\Omega+\omega)t}{2}$ for the initial state $|\psi(t=0)\rangle = |gg\rangle$. The corresponding time average values are $\bar{P}_{gg} = \bar{P}_{rr} = 0.375$, $\bar{P}_{gr} = \bar{P}_{rg} = 0.125$ for $\omega = 0$ and $\bar{P}_{gg} = \bar{P}_{rr} = \bar{P}_{gr} = \bar{P}_{rg} = 0.25$ for $\omega \neq 0$. The effect of a nonzero ω on the time average populations at $V_0 = 0$ has an influence as well as when

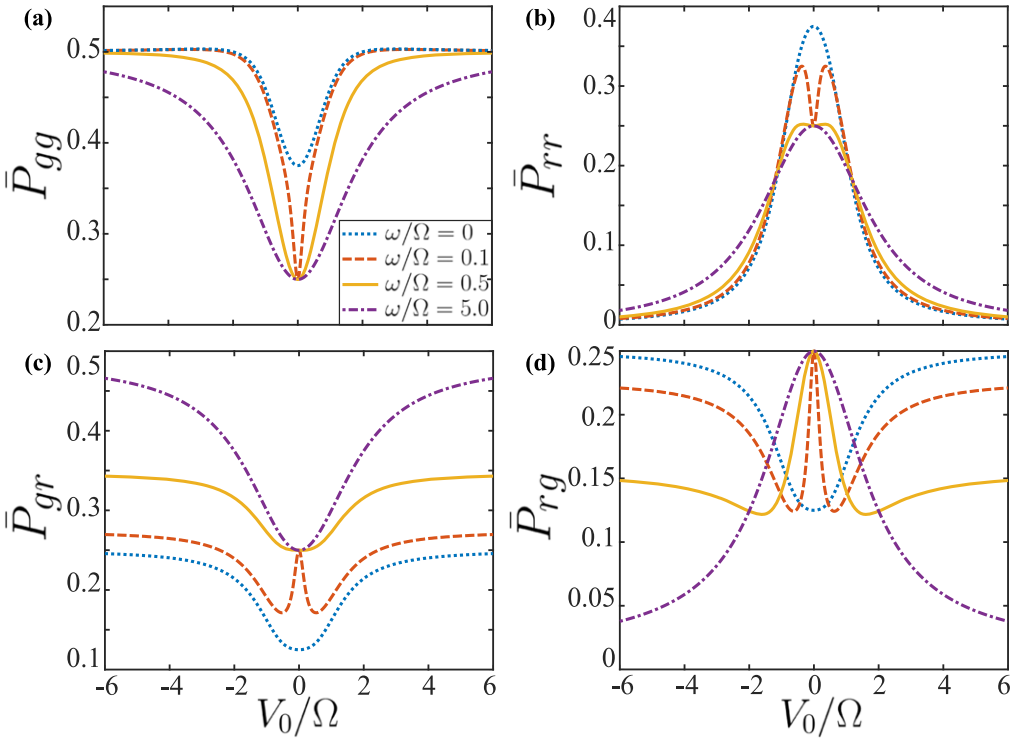

Figure 4. The time average populations: (a) $\bar{P}_{gg}$, (b) $\bar{P}_{rr}$, (c) $\bar{P}_{gr}$ and (d) $\bar{P}_{rg}$ as a function of V_0/Ω for different ω/Ω, with $\Delta = \delta = 0$, $|\psi(t=0)\rangle = |gg\rangle$ and $\Omega\tau = 5000$. For very small values of ω/Ω, the populations $\bar{P}_{rr}$, $\bar{P}_{rg}$ and $\bar{P}_{gr}$ depend non-monotonously on $|V_0|$.

$V_0 \neq 0$, and qualitatively noticeable especially, at small ω and V_0 as seen in figure 4.

As previously mentioned, when $\omega = 0$ and $V_0 \neq 0$, the population is transferred from $|gg\rangle$ to $|rr\rangle$ state via the entangled state $|+\rangle$, thus preserving the exchange symmetry between the two atoms at any instant, and $\bar{P}_{rr}$ decreases monotonously with increasing $|V_0|$ whereas $\bar{P}_{gg}$ and $\bar{P}_{+}$ increases and saturates to 0.5 at large $|V_0|$. As soon as $\omega \neq 0$, the symmetry is broken, resulting in $\bar{P}_{gr} \neq \bar{P}_{rg}$ and as expected, $\bar{P}_{gr}$ gets larger with larger ω for any $V_0 \neq 0$. As seen in figure 4(b) (also in figure 2(b)), for small values of ω, $\bar{P}_{rr}$ exhibits a non-monotonous behaviour as a function of $|V_0|$. For $\omega = 0$, we get a single Lorentzian profile of $\bar{P}_{rr}$ centered at $V_0 = 0$. However, for small values of ω, the single Lorentzian undergoes a partial splitting, exhibiting two peaks at $\pm V_0^p$ around $V_0 = 0$. This arises from the competition between the terms associated with V_0 and ω in equation (3) for small values of V_0 and ω. This is also evident from the plots of $\bar{P}_{gr}$, $\bar{P}_{rg}$, and $\bar{P}_{gg}$ shown in figure 4. Focusing on $\bar{P}_{rr}$ (figure 2(b)), for very small ω such that $\bar{P}_{gr} \approx \bar{P}_{rg}$, increasing $|V_0|$ from zero suppresses the effect of the offset ω, leading to the recovery of $\bar{P}_{rr}$ to the value obtained for $\omega = 0$. Once $|V_0|$ dominates, $\bar{P}_{rr}$ starts to decrease as expected from the blockade effect. As a result, the peaks separation ($2V_0^p$) increases with increasing ω until it reaches a value for ω such that V_0 can no longer nullify the effect of ω, see figure 5(a). At that point, there is a substantial difference between the magnitudes of $\bar{P}_{gr}$ and $\bar{P}_{rg}$, and V_0^p decreases with further increase in ω, reaches zero. Thus, when ω becomes greater than a particular value, the population $\bar{P}_{rr}$ becomes a Lorentzian function of V_0. The peak separation follows, $V_0^p \propto \sqrt{\omega}$ for small values of ω. The width of the Lorentzian ν_{rr} as a function of ω is shown in figure 5(b). The shaded region for small ω in figure 5(b) indicates the existence of a double-peak structure, and ν_{rr} saturates to a constant value at large values of ω. The latter also indicates that the blockade condition is not affected by ω at large values of ω, as we have discussed above. In section 4, using an effective Hamiltonian obtained in the limit $\{\omega, V_0\} \ll \Omega$, we explain the initial increment of $\bar{P}_{rr}$ in V_0 at small ω and also the same is done in appendix A using the second-order perturbation theory obtained in the weak interaction limit. Alternatively, one could also think, the peaks in $\bar{P}_{rr}$ vs V_0 emerge as a consequence of quantum interference since both ω and V_0 introduce additional phase shifts in the amplitudes of quantum paths populating the state $|rr\rangle$. Note that the emergent splitting of $\bar{P}_{rr}$ in the V_0 axis has a resemblance to the Autler-Townes effect, but here using two particle states and also consequently the antiblockade effect [66].

4. Effective Hamiltonians

At this point, we obtain the effective Hamiltonians describing the long-time behaviour of our setup in different limits. First we consider the limit of $V_0 \gg \{\Omega, \omega\}$ and we introduce the unitary transformation, $\hat{U} = \exp(iV_0\hat{\sigma}_{rr}^1\hat{\sigma}_{rr}^2 t)$ to the Hamiltonian in equation (3). The new Hamiltonian,

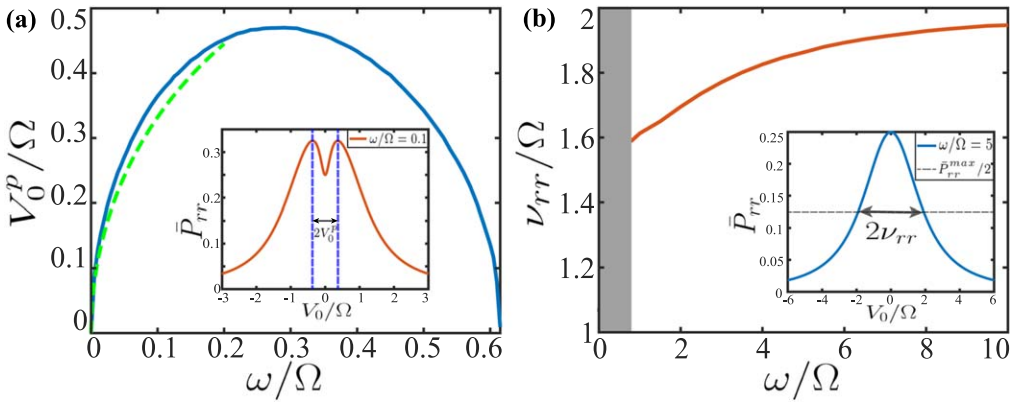

Figure 5. (a) The half of the peak separation V_0^P in $\bar{P}_{rr}$ (see inset) as a function of ω/Ω. The dashed line is the analytical result given by equation (27) obtained for small ω. (b) shows the Lorentzian width (ν_{rr}) of $\bar{P}_{rr}$ as a function of ω/Ω. The width is obtained at the half-maximum of $\bar{P}_{rr}$ distribution in V_0/Ω. The shaded region for small ω indicates the existence of double peak structure in $\bar{P}_{rr}$ shown in the inset of (a).

$\hat{H}' = \hat{U}\hat{H}\hat{U}^\dagger + i(d\hat{U}/dt)\hat{U}^\dagger$ is

$$\hat{H}' = \frac{\Omega}{2}[|gg\rangle\langle gr| + |gg\rangle\langle rg| + e^{-iV_0t}(|gr\rangle\langle rr| + |rg\rangle\langle rr|) + \text{H.c.}] + \frac{\omega}{2}(|gg\rangle\langle gr| + |rg\rangle\langle rr|e^{-iV_0t} + \text{H.c.}) \quad (8)$$

In the second step, we obtain a period average Hamiltonian, $\hat{H}_{eff}^{(V_0)} = (1/T)\int_0^T H'(t)dt$, with time period $T = 2\pi/V_0$, which provides us with

$$\hat{H}_{eff}^{(V_0)} = \frac{(\omega+\Omega)}{2}\hat{\sigma}_{gg}^1\hat{\sigma}_x^2 + \frac{\Omega}{2}\hat{\sigma}_x^1\hat{\sigma}_{gg}^2. \quad (9)$$

The second step is identical to removing the fast oscillations emerging from large V_0. Even after integrating out the interaction dependent terms, still the effective Hamiltonian $\hat{H}_{eff}^{(V_0)}$ cannot be written as a sum of two single particle terms, indicating the existence of quantum correlations between the two atoms, which we quantify later. The first term in equation (9) leaves the first atom in the ground state while driving the second atom with a Rabi coupling $\omega + \Omega$, and is vice versa for the second term but with a Rabi coupling Ω for the first atom. The two terms, being the correlated Rabi couplings [67], are also identical to the density assisted interband tunneling for atoms in optical lattices [68]. When $\omega \gg \Omega$, the second term in equation (9) is merely a perturbation to the first term, leading to the scenario of Rydberg-biased freezing. In the effective Hamiltonian $\hat{H}_{eff}^{(V_0)}$ in equation (9), we see that the basis gets truncated to $\{|gg\rangle, |gr\rangle, |rg\rangle\}$. This happens because, in the large V_0 limit, the $|rr\rangle$ state only gets minimally populated due to Rydberg blockade. By using the effective Hamiltonian in the Schrödinger equation, we can explicitly obtain the time-dependent populations as,

$$P_{gg}(t) = \cos^2\beta t \quad (10)$$

$$P_{gr}(t) = \left(\frac{\Omega+\omega}{2\beta}\right)^2 \sin^2\beta t \quad (11)$$

$$P_{rg}(t) = \left(\frac{\Omega}{2\beta}\right)^2 \sin^2\beta t, \quad (12)$$

where $\beta^2 = [(\Omega+\omega)^2 + \Omega^2]/4$. Note that, at $t = 0$, $\hat{U}(0) = \mathcal{I}$, the identity operator that leaves the initial state unchanged is also same for the different transformations we consider below. The time average populations become $\bar{P}_{gg} = 1/2$, $\bar{P}_{gr} = [(\Omega+\omega)/2\beta]^2/2$ and $\bar{P}_{rg} = (\Omega/2\beta)^2/2$. From equations (11) and (12) we can see that for $\omega \ll \Omega$, we have $\bar{P}_{gr} \approx \bar{P}_{rg}$, which is consistent with numerical results shown in figure 2. For $\omega \gg \Omega$ we have $P_{gr}(t) \approx \sin^2\beta t$ with $\beta \approx \omega/2$, indicating the Rabi oscillations between the states $|gg\rangle$ and $|gr\rangle$ with a Rabi frequency approximately ω. We compare these results with the numerical solutions obtained by solving the full Hamiltonian in equation (3),and is found to be in an excellent agreement when $V_0 \gg \Omega$ (see figure 3(b)).

Now we derive the effective Hamiltonian in the limit $\omega \gg \{\Omega, V_0\}$ by doing a similar procedure as above. For that we introduce a local unitary operator $\hat{U} = \exp(i\omega\hat{\sigma}_x^{i=2}t/2)$ acting only on the second atom, which gives us the new Hamiltonian

$$\hat{H}' = \frac{\Omega}{2}\sum_{i=1}^{2}\hat{\sigma}_x^i + V_0\left(\frac{1-\cos\omega t}{2}\hat{\sigma}_{rr}^1\hat{\sigma}_{gg}^2 + \frac{1+\cos\omega t}{2}\hat{\sigma}_{rr}^1\hat{\sigma}_{rr}^2 - \frac{\sin\omega t}{2}\hat{\sigma}_{rr}^1\hat{\sigma}_y^2\right), \quad (13)$$

and then averaging over a time period of $T = 2\pi/\omega$, we get

$$\hat{H}_{eff}^{(\omega)} = \frac{\Omega}{2}\sum_{i=1}^{2}\hat{\sigma}_x^i + \frac{V_0}{2}\hat{\sigma}_{rr}^1. \quad (14)$$

The effective Hamiltonian $\hat{H}_{eff}^{(\omega)}$ can be written as a sum of two single particle Hamiltonians, with an effective detuning $V_0/2$ for the first atom. Note that, in the new rotating frame, the Rabi coupling of the second atom is reduced to Ω. From $\hat{H}_{eff}^{(\omega)}$ it is clear that, for $V_0 \gg \Omega$, the first atom is merely excited resulting in the Rydberg-biased freezing and also indicates

that the two atom correlations get suppressed in the large ω limit (see section 5).

Finally, we consider the limit $\{V_0, \omega\} \ll \Omega$, and introducing the unitary operator $\hat{U} = e^{i\frac{\Omega}{2}(\hat{\sigma}_x^1+\hat{\sigma}_x^2)t}$ we obtain,

$$\begin{aligned}\hat{H}' = &\frac{V_0}{4}[(\cos\Omega t - 1)^2 |gg\rangle\langle gg| + (\cos\Omega t + 1)^2 |rr\rangle\langle rr| \\ &+ \sin^2\Omega t((|gr\rangle\langle gr| + |rg\rangle\langle rg|) + (|gr\rangle\langle rg| + \text{ H.c.})) \\ &+ (\cos^2\Omega t - 1)(|gg\rangle\langle rr| + \text{H.c.})] + \frac{\omega}{2}\hat{\sigma}_x^2 \\ &+ \left[\frac{iV_0\sin\Omega t}{4}(1 - \cos\Omega t)(|gg\rangle\langle gr| + |gg\rangle\langle rg|) + \text{H.c.}\right] \\ &+ \left[\frac{iV_0\sin\Omega t}{4}(1 + \cos\Omega t)(|gr\rangle\langle rr| + |rg\rangle\langle rr|) + \text{H.c.}\right].\end{aligned} \tag{15}$$

Then, the effective Hamiltonian after averaging over $T = 2\pi/\Omega$, in the basis $\{|gg\rangle, |gr\rangle, |rg\rangle, |rr\rangle\}$:

$$\hat{H}_{eff}^{(\Omega)} = \begin{bmatrix} 3V_0/8 & \omega/2 & 0 & -V_0/8 \\ \omega/2 & V_0/8 & V_0/8 & 0 \\ 0 & V_0/8 & V_0/8 & \omega/2 \\ -V_0/8 & 0 & \omega/2 & 3V_0/8 \end{bmatrix}, \tag{16}$$

and together with the basis vectors transformations

$$\begin{aligned}\hat{U}|gg\rangle &= \cos^2\frac{\Omega t}{2}|gg\rangle + \frac{i\sin\Omega t}{2}(|gr\rangle + |rg\rangle) - \sin^2\frac{\Omega t}{2}|rr\rangle \\ \hat{U}|gr\rangle &= \frac{i\sin\Omega t}{2}(|gg\rangle + |rr\rangle) + \cos^2\frac{\Omega t}{2}|gr\rangle - \sin^2\frac{\Omega t}{2}|rg\rangle \\ \hat{U}|rg\rangle &= \frac{i\sin\Omega t}{2}(|gg\rangle + |rr\rangle) - \sin^2\frac{\Omega t}{2}|gr\rangle + \cos^2\frac{\Omega t}{2}|rg\rangle \\ \hat{U}|rr\rangle &= -\sin^2\frac{\Omega t}{2}|gg\rangle + \frac{i\sin\Omega t}{2}(|gr\rangle + |rg\rangle) + \cos^2\frac{\Omega t}{2}|rr\rangle,\end{aligned} \tag{17}$$

we can estimate the time average populations at small ω and V_0. For instance, when $V_0 = \omega = 0$ and with the initial state in the rotating frame, $|\psi_R(t=0)\rangle = \hat{U}|\psi(t=0)\rangle = |gg\rangle$, the time average populations can be estimated directly from $\hat{U}|gg\rangle$, which gives us $\bar{P}_{gg} = \bar{P}_{rr} = 0.375$ and $\bar{P}_{gr} = \bar{P}_{rg} = 0.125$, as expected. But, when either $\omega \neq 0$ or $V_0 \neq 0$, we need to first use the Hamiltonian evolution of $\hat{H}_{eff}^{(\Omega)}$. Taking $V_0 = 0$ and $\omega \neq 0$, in the rotating frame, the initial $|gg\rangle$ state undergoes coherent Rabi oscillations with $|gr\rangle$ according to $\hat{H}_{eff}^{(\Omega)}$, i.e., $|\psi_R(t)\rangle = \cos\frac{\omega t}{2}|gg\rangle - i\sin\frac{\omega t}{2}|gr\rangle$. Then, the population in $|rr\rangle$ state is obtained by projecting $|\psi_R(t)\rangle$ along $\hat{U}|rr\rangle$. The latter provides us with the same result discussed in section 3. Now, we take $\omega = 0$ and $V_0 \neq 0$, but $V_0 \ll \Omega$. The $\hat{H}_{eff}^{(\Omega)}$ results in $|\psi_R(t)\rangle = \left[\cos\frac{V_0 t}{8}|gg\rangle + i\sin\frac{V_0 t}{8}|rr\rangle\right]\exp(-i3V_0 t/8)$ and then projecting onto the rotated basis states given in equations (17), we get for $\omega = 0$ and $V_0 \ll \Omega$:

$$P_{gg}(t) = \cos^4\frac{\Omega t}{2}\cos^2\frac{V_0 t}{8} + \sin^4\frac{\Omega t}{2}\sin^2\frac{V_0 t}{8} \tag{18}$$

$$P_{gr}(t) = P_{rg}(t) = \frac{1}{4}\sin^2\Omega t \tag{19}$$

$$P_{rr}(t) = \cos^4\frac{\Omega t}{2}\sin^2\frac{V_0 t}{8} + \sin^4\frac{\Omega t}{2}\cos^2\frac{V_0 t}{8}. \tag{20}$$

These results are in excellent agreement with the numerical results obtained by solving the Schrödinger equation using the Hamiltonian in equation (3) when $V_0 \ll \Omega$ is satisfied. For both ω and V_0 are non zero but very small compared to Ω, it is clear from the effective Hamiltonian in equation (16) that a competition between V_0 and ω exists in coupling the state $|gg\rangle$ to other states, as we have already discussed in section 3. With the initial $|gg\rangle$ state, the unitary evolution of $H_{eff}^{(\Omega)}$ results in

$$\begin{aligned}|\Psi_R(t)\rangle = e^{-iV_0 t/4} \times \Bigg[&\frac{1}{2\eta}(\eta(\cos\omega t/2 + \cos\eta t/4) \\ &- iV_0\sin\eta t/4)|gg\rangle \\ &- \frac{i}{4\omega\eta}(\eta^2\sin\eta t/4 + 2\omega\eta\sin\omega t/2 - V_0^2\sin\eta t/4)|gr\rangle \\ &+ \frac{i}{4\omega\eta}(\eta^2\sin\eta t/4 - 2\omega\eta\sin\omega t/2 - V_0^2\sin\eta t/4)|rg\rangle \\ &- \frac{1}{2\eta}(\eta(\cos\eta t/4 - \cos\omega t/2) - iV_0\sin\eta t/4)|rr\rangle\Bigg],\end{aligned} \tag{21}$$

and then projecting to the rotated basis states given in equations (17) we get for $\{V_0, \omega\} \ll \Omega$

$$P_{gg}(t) = \frac{1}{4}\left(\cos\frac{(\omega+2\Omega)t}{2} + \cos\frac{\eta t}{4}\right)^2 + \frac{V_0^2}{4\eta^2}\sin^2\frac{\eta t}{4} \tag{22}$$

$$P_{gr}(t) = \left(\frac{1}{2}\sin\frac{(\omega+2\Omega)t}{2} + \frac{\omega}{\eta}\sin\frac{\eta t}{4}\right)^2 \tag{23}$$

$$P_{rg}(t) = \left(\frac{1}{2}\sin\frac{(\omega+2\Omega)t}{2} - \frac{\omega}{\eta}\sin\frac{\eta t}{4}\right)^2 \tag{24}$$

$$P_{rr}(t) = \frac{1}{4}\left(\cos\frac{(\omega+2\Omega)t}{2} - \cos\frac{\eta t}{4}\right)^2 + \frac{V_0^2}{4\eta^2}\sin^2\frac{\eta t}{4} \tag{25}$$

where $\eta = \sqrt{V_0^2 + 4\omega^2}$. The time average values become

$$\bar{P}_{gg} = \bar{P}_{rr} = 1/4 + V_0^2/(8\eta^2), \tag{26}$$

and $\bar{P}_{gr} = \bar{P}_{rg} = 1/8 + \omega^2/(2\eta^2)$. When $\omega = 0$, we retrieve the old results. For $\omega \neq 0$, $\bar{P}_{rr}$ is an increasing function of V_0 which explains why $\bar{P}_{rr}$ increases initially with $|V_0|$ at small values of ω. The saturation point V_0^P shown in figure 5(a) for small ω can be obtained by equating the $\bar{P}_{rr}$ given in equation (26) to the Lorentzian profile, $f(V_0/\Omega) = 3\Omega^2/8[\Omega^2 + (V_0/\nu_{rr})^2]$, obtained for $\bar{P}_{rr}$ with $\omega = 0$, in which ν_{rr} is obtained by fitting to the exact numerical results. Doing so, we get

$$V_0^p = \sqrt{\frac{2}{3}}\sqrt{\omega(-2\omega + \sqrt{4\omega^2 + 3\nu_{rr}^2\Omega^2})}, \tag{27}$$

which is shown as a dashed line in figure 5(a). A comparison of time average populations from exact numerics, perturbation theory (appendix A) and using the effective Hamiltonian is shown in figure 6 for small values of ω/Ω and V_0/Ω, and they are in good agreement with each other.

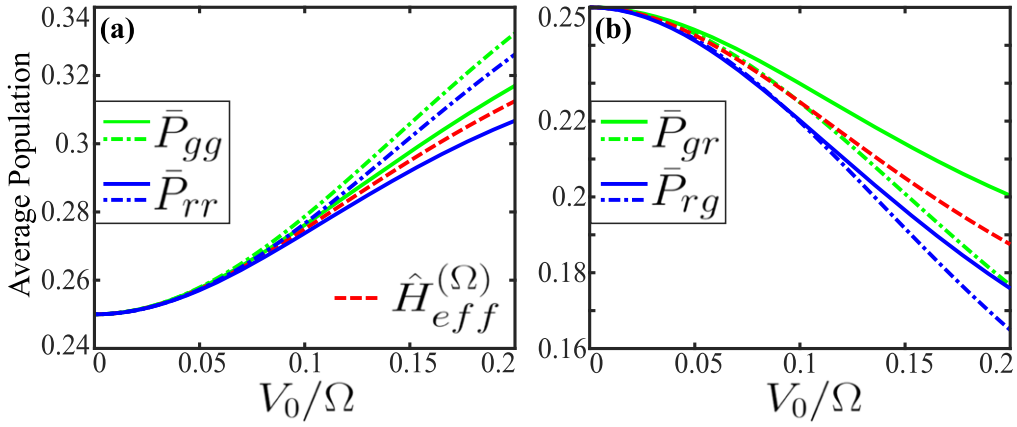

Figure 6. Comparison of results from three different methods: exact numerical solution (solid lines), perturbation theory (dotted-dashed lines) for weak interactions and using the effective Hamiltonian $\hat{H}^{(\Omega)}_{eff}$ (dashed line) for $\omega/\Omega = 0.1$. (a) is for the time average populations $\bar{P}_{gg}$ and $\bar{P}_{rr}$ and (b) is for $\bar{P}_{gr}$ and $\bar{P}_{rg}$.

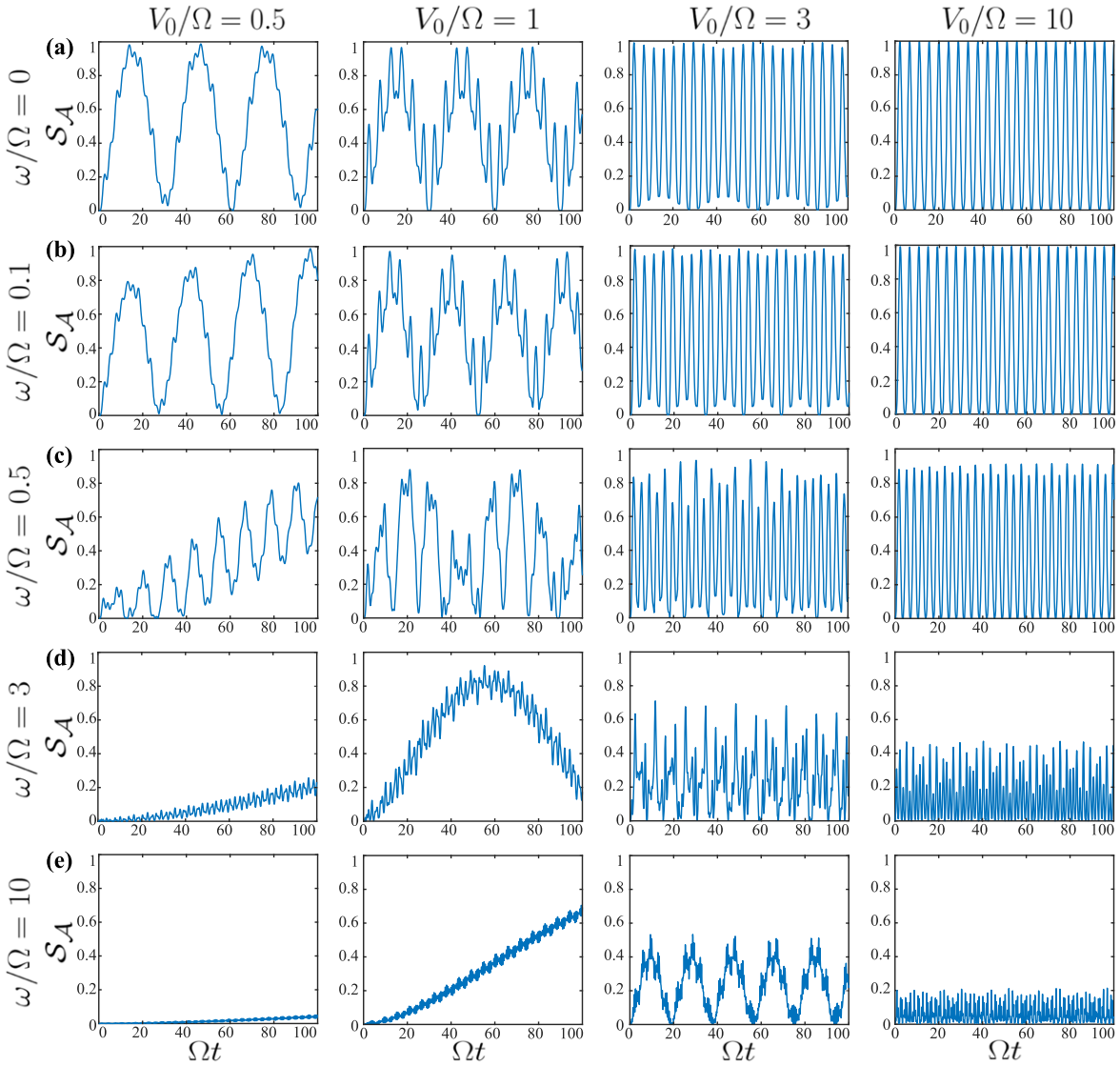

Figure 7. (a)–(e) The time evolution of the entanglement entropy $\mathcal{S}_A(t)$ obtained from the reduced density matrix of the first atom for different ω/Ω and V_0/Ω corresponding to the coherent dynamics discussed in section 3. In this case $\mathcal{S}_A$ is same as the discord $\mathcal{D}$. The values of ω/Ω and V_0/Ω are indicated in the left and top sides respectively.

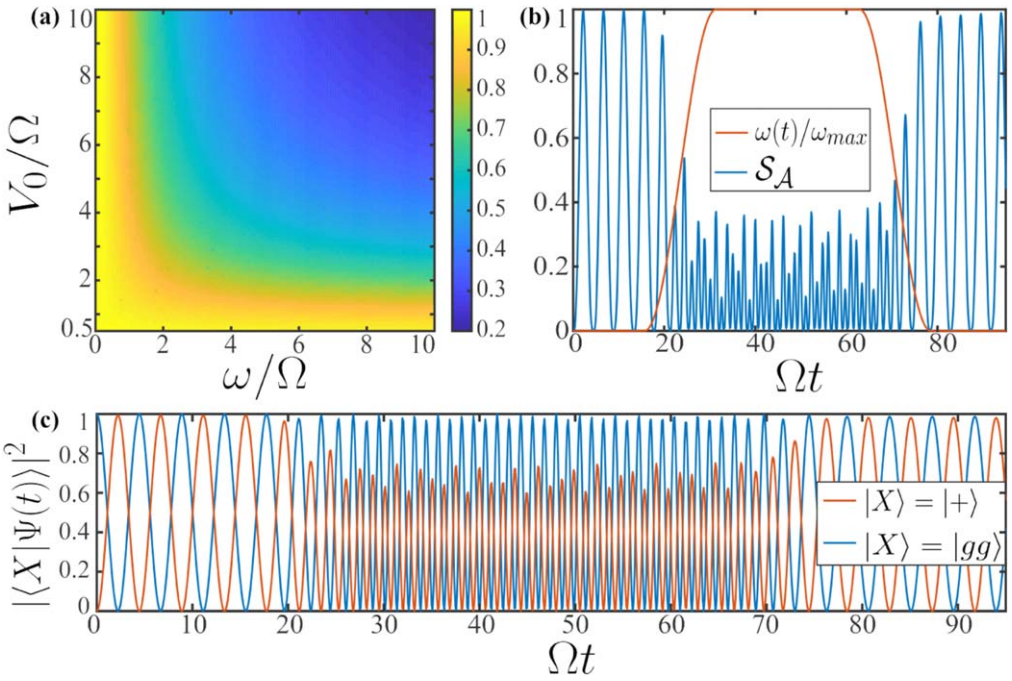

Figure 8. (a) The maximum of $\mathcal{S}_A(t)$ as a function of ω/Ω and V_0/Ω corresponding to the coherent dynamics discussed in section 3. The lower cutoff of $V_0/\Omega = 0.5$ in the vertical axis is because for smaller values, the time taken to attain maximum $\mathcal{S}_A(t)$ becomes extremely large. (b) The dynamics of $\mathcal{S}_A(t)$ when the Rabi-offset ω is varied in time with $\alpha = 0.1\Omega$ (see text), $V_0/\Omega = 10$ and $\omega_{\max}/\Omega = 4$. When ω reaches the maximum, $\mathcal{S}_A(t)$ is significantly suppressed, and is retrieved back to the initial dynamics once ω is brought back to zero. (c) shows the overlap of $|\psi(t)\rangle$ on the states $|gg\rangle$ and $|+\rangle$ for the dynamics shown in (b).

5. Quantum correlations: entanglement entropy

In this section, we analyze the growth and subsequent evolution of the entanglement entropy $\mathcal{S}_A$ for the coherent dynamics discussed in section 3. At $t = 0$, we have $\mathcal{S}_A(0) = 0$ since the initial state $|gg\rangle$ is a separable state. Figure 7 shows $\mathcal{S}_A(t)$ for different values of V_0/Ω and ω/Ω and, is an oscillating function of time. Each row of four plots is for a fixed ω/Ω and different V_0/Ω, and vice versa for the columns. For $V_0 = 0$, there is no correlation ($\mathcal{S}_A = 0$) between the atoms. When $\omega = 0$ and for any interaction strengths ($|V_0| \neq 0$), $\mathcal{S}_A(t)$ oscillates between 0 and its maximum possible value of $\log_2 2 = 1$. The larger the value of V_0, the maximum correlation is attained between shorter intervals of time. For sufficiently large V_0, $\mathcal{S}_A(t)$ exhibits clean periodic oscillation between 0 and 1, indicating a complete blockade in which the system exhibits coherent Rabi oscillations between the separable $|gg\rangle$ state and a maximally entangled $|+\rangle$ state. Making $\omega \neq 0$ significantly changes the growth and dynamics of the quantum correlations depending on the value of V_0. Not only does ω slow down the correlation growth but also lowers the maximum correlation that can be attained. When both ω and V_0 are very large compared to Ω, the correlations are very well suppressed due to the Rydberg-biased freezing (see figure 7). For sufficiently small V_0, increasing ω slowed down the growth of $\mathcal{S}_A(t)$ but did not affect the maximum value of $\mathcal{S}_A$ attained over time (see along the first column in figure 7 and also figure 8(a) in which the maximum of $\mathcal{S}_A(t)$ is shown). It indicates that ω effectively reduces the effect of interaction strengths between the two atoms for small V_0 or in other words, a competition between V_0 and ω exists, as we pointed out earlier in sections 3 and 4. The maximum value of $\mathcal{S}_A(t)$ as a function of V_0/Ω and ω/Ω is shown in figure 8(a). We introduced a lower cutoff for V_0 in the vertical axis in figure 8(a) since the time taken to attain the maximum correlation becomes extremely large for such small values of V_0 with large ω.

The above results opens up the possibility that the quantum correlations between the two atoms can be easily controlled by means of the Rabi-offset. To demonstrate that, we consider a time-dependent ω (see figure 8(b)) as follows:

$$\omega(t)/\omega_{\max} = \begin{cases} 0, & 0 \leqslant \alpha t \leqslant \pi/2 \\ \cos^2(\alpha t), & \pi/2 \leqslant \alpha t \leqslant \pi \\ 1, & \pi \leqslant \alpha t \leqslant 2\pi \\ \cos^2(\alpha t), & 2\pi \leqslant \alpha t \leqslant 5\pi/2 \\ 0, & 5\pi/2 \leqslant \alpha t \leqslant 3\pi \end{cases} \tag{28}$$

where α determines the rate at which ω is varied. We take sufficiently large V_0 such that the two-atom setup is in the fully blockade region, thus $\mathcal{S}_A(t)$ exhibits periodic oscillation between 0 and 1 in the absence of any Rabi-offset. Starting from the initial state $|gg\rangle$, first we slowly ramp $\omega(t)$ to $\omega_{\max}$. The $\omega(t)$ suppresses the population in $|rg\rangle$ and consequently in $|+\rangle$ state (see figure 8(c)). The latter results in a significant loss of quantum correlations between the atoms. As we reduce $\omega(t)$ back to zero, the correlations are again built up in the system and completely retrieve its maximum value of 1 as ω vanishes. In the example shown in figures 8(b) and (c), the value of α is taken such that not only the correlations are

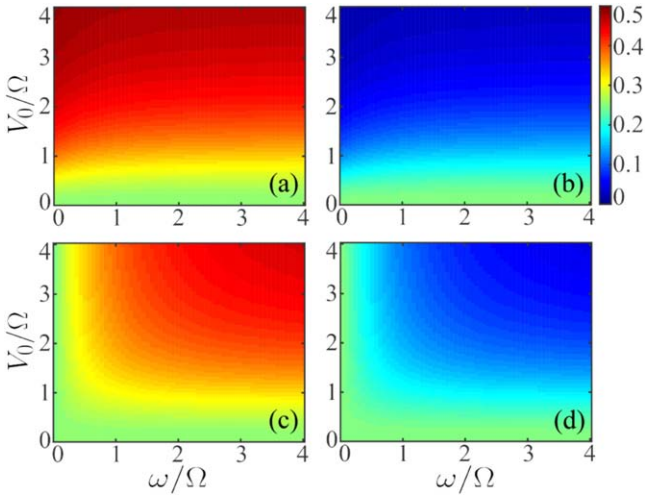

Figure 9. The steady state populations: (a) ρ_{gg}, (b) ρ_{rr}, (c) ρ_{gr} and (d) ρ_{rg} as a function of ω/Ω and V_0/Ω with $\Gamma/\Omega = 0.1$.

rebuilt, but also the initial blockade dynamics is retrieved completely. The latter is verified by calculating the overlap functions $|\langle X|\psi(t)\rangle|^2$ where $|X\rangle \in \{|gg\rangle, |+\rangle\}$, see figure 8(c).

6. Dissipative dynamics: steady states and quantum discord

At this point, we discuss the effect of spontaneous emission from the Rydberg state $|r\rangle$ on the dynamics as well as the steady-state quantum discord by solving the master equation in equation (6). Since the dissipation drives the system into a mixed state, entanglement entropy is no longer a good measure for quantum correlations [50, 64, 65], and we restrict ourselves to quantum discords. As stated before, for a mixed state, $\mathcal{D}(A:B)$ may not be always equal to $\mathcal{D}(B:A)$ (figure 11). In our two atoms setup with an initial state $\rho_{gg} = 1$, $\mathcal{D}(A:B) = \mathcal{D}(B:A)$ only when $\omega = 0$, due to the exchange symmetry between the atoms. Since the initial state is a product state, we have vanishing discords at $t = 0$. In addition to discord, more insights into the steady states can be attained from the purity of the system and the subsystems (figures 10(a)–(c)). The quantity $\mathrm{Tr}\,(\hat{\rho}_{AB}^2)$ measures the purity of the total system, and $\mathrm{Tr}\,(\hat{\rho}_A^2)$ $[\mathrm{Tr}\,(\hat{\rho}_B^2)]$ measures that of the subsystem A $[B]$. As we see below, we have $\mathcal{D}(B:A) > \mathcal{D}(A:B)$ since the purity of $\hat{\rho}_A$ remains larger than $\hat{\rho}_B$ at any instant.

The steady state populations ρ_{gg}, ρ_{gr}, ρ_{rg}, and ρ_{rr} as a function of ω/Ω and V_0/Ω with $\Gamma/\Omega = 0.1$ is shown in figure 9. Two features are directly evident from figure 9(b): (i) the doubly excited state (ρ_{rr}) is completely suppressed at large V_0 due to the blockade, and (ii) for sufficiently large ω the blockade criteria is independent of ω similar to that in the case of coherent dynamics. In the blockade regime with very small ($\omega \ll \Omega$) we have $\rho_{gg} \sim 0.5$ and $\rho_{gr} \approx \rho_{rg} \sim 0.25$ at the steady state. At sufficiently large values of V_0 and ω, both ρ_{rr} (figure 9(b)) and ρ_{rg} (figure 9(d)) approaches zero and the populations are shared among ρ_{gg} (figure 9(a)) and ρ_{gr} (figure 9(c)), which is consistent with the results in the coherent case and thus Rydberg-biased freezing is robust against dissipation.

For small values of $V_0 (\ll \Omega)$, independent of the value of ω, at the steady state the total system $[\mathrm{Tr}\,(\hat{\rho}_{AB}^2) \sim 0.25]$ as well as the subsystems $[\mathrm{Tr}\,(\hat{\rho}_A^2) \sim 0.5$ and $\mathrm{Tr}\,(\hat{\rho}_B^2) \sim 0.5]$ are completely mixed with no quantum correlations between the subsystems; see figure 11 for the corresponding discords. Thus, the steady state of the system is a product state, $\rho_{AB} = \rho_A \otimes \rho_B$ and consequently $\mathrm{Tr}\,(\hat{\rho}_{AB}^2) = \mathrm{Tr}\,(\hat{\rho}_A^2) \times \mathrm{Tr}\,(\hat{\rho}_B^2)$. In otherwords, for sufficiently small V_0, the correlations that initially build up in the system from the interaction between the subsystems have been washed out eventually by the dissipation.

As V_0 increases $\mathrm{Tr}\,(\hat{\rho}_{AB}^2)$ increases and saturates to a value of 0.5 in the blockade region. Interestingly, the latter happens independent of the value of ω (figure 10(c)), but a complete picture is accessible only through $\mathrm{Tr}\,(\rho_A^2)$ and $\mathrm{Tr}\,(\rho_B^2)$. For instance, the purity as a function of ω/Ω in the blockade region ($V_0/\Omega = 10$) is shown in figure 10(d). Though $\mathrm{Tr}\,(\rho_{AB}^2) \sim 0.5$ is independent of ω at large V_0, the purity of the subsystems depends strongly on ω/Ω as shown in figures 10(a)–(b). The purity in the strongly driven atom (subsystem B) decreases as a function of ω/Ω and becomes maximally mixed at sufficiently large values, whereas that of the first atom (subsystem A) increases with ω and eventually becomes a pure state at very large values of ω/Ω. Thus, the total system is in a product state for large V_0 and ω, and the purity of the system becomes $\mathrm{Tr}\,(\hat{\rho}_{AB}^2) = \mathrm{Tr}\,(\hat{\rho}_A^2) \times \mathrm{Tr}\,(\hat{\rho}_B^2)$ as shown in figure 10(d).

Concerning the quantum discord, when V_0 increases, for sufficiently small ω, the correlations survive in the steady state as shown in figure 11, and their magnitude increases with an increase in V_0, and eventually saturates to a constant value (Γ-dependent) at large values of $V_0 (\sim 10\Omega)$. The strong correlations at large V_0 for small ω is attributed to the Rydberg blockade [60]. The maximum quantum discord possessed by the system at large V_0 decreases with an increase in the rabi-offset ω as shown in figure 10(d), similar as in the case of the coherent dynamics discussed in section 5.

Since, Rydberg-biased freezing is one of the main features in our studies, we explicitly discuss the dissipative dynamics in that regime, see figure 12. In figure 12(a), we show the time evolution of the populations $[\rho_{\alpha\beta}(t)$ with α, $\beta \in \{g, r\}]$ for $\omega/\Omega = V_0/\Omega = 5$ and $\Gamma/\Omega = 0.1$. At shorter times we see the damped Rabi oscillations between the states $|gg\rangle$ and $|gr\rangle$ (inset of figure 12(a)) whereas the states $|rg\rangle$ and $|rr\rangle$ are almost suppressed. Eventually, the system reaches the steady state with almost equal populations between $|gg\rangle$ and $|gr\rangle$. Figure 12(b) shows the corresponding dynamics of both the quantum discord and the purity as a function of time. Note that $\mathrm{Tr}\,(\hat{\rho}_A^2)$ remains close to unity during the dissipative evolution with small fluctuations initially, and becomes steady at unity as the system converges to the steady state. This makes sense, because the first atom remains frozen in the ground state due to the Rydberg-biased freezing and thus, in a

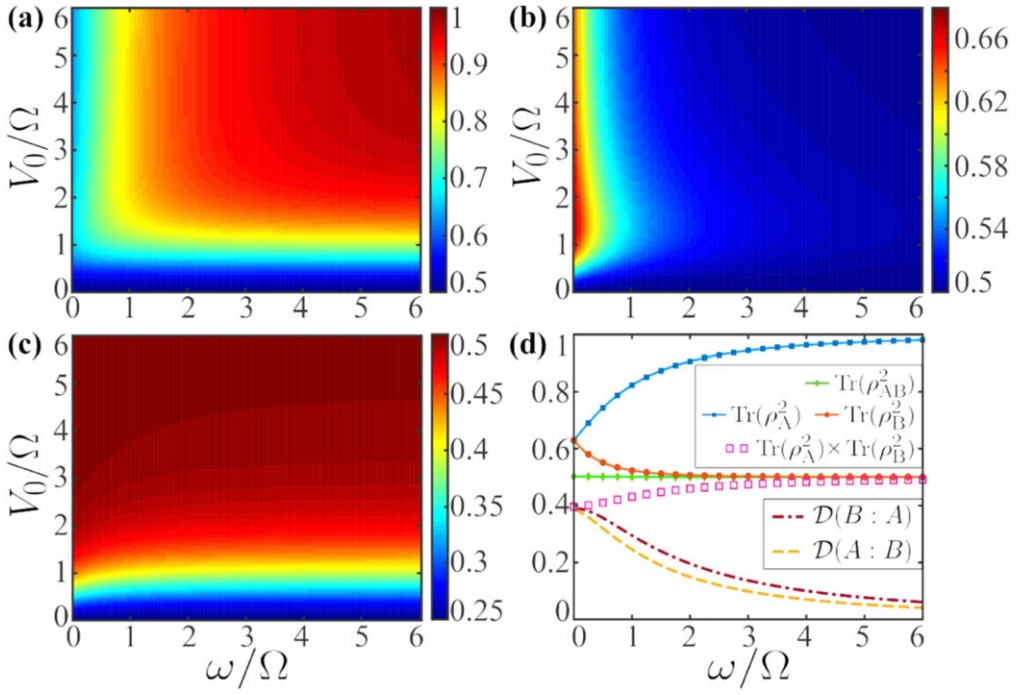

Figure 10. The steady state purity of the subsystems (a) A and (b) B, and (c) the full system (AB) as a function of ω/Ω and V_0/Ω. (d) shows the purity and the quantum discords as a function of ω/Ω for $V_0/\Omega = 10$ (blockade region). $\Gamma/\Omega = 0.1$ for all figures. In (d) the solid lines are the analytical results given in appendix B and points are from the full numerical calculations for the steady state purity. Dashed lines show the quantum discords. The open squares show $\mathrm{Tr}\,(\hat{\rho}_A^2) \times \mathrm{Tr}\,(\hat{\rho}_B^2)$ which matches to $\mathrm{Tr}\,(\hat{\rho}_{AB}^2)$ at large ω.

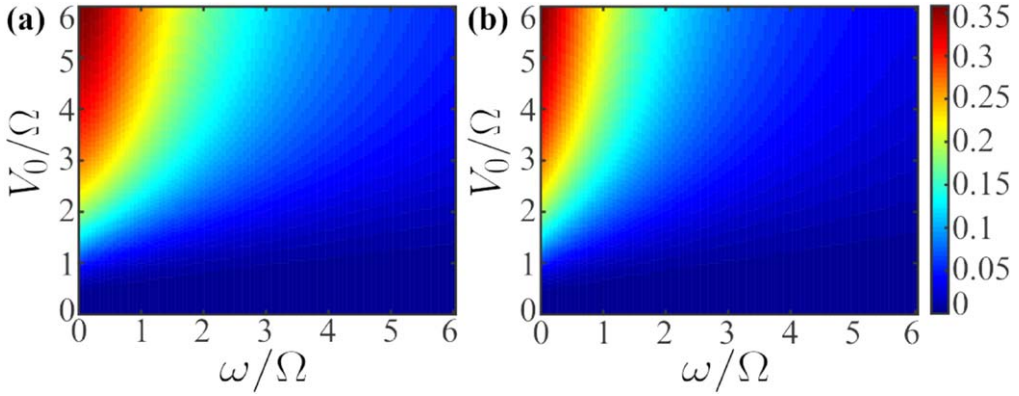

Figure 11. The steady state quantum discords (a) $\mathcal{D}(B:A)$ and (b) $\mathcal{D}(A:B)$ as a function of ω/Ω and V_0/Ω for $\Gamma/\Omega = 0.1$. For $\omega \neq 0$ we have $\mathcal{D}(B:A) \neq \mathcal{D}(A:B)$. For $\omega = 0$, the correlations maximally saturate at large V_0 due to blockade, and they start to diminish as ω increases. Discords vanish in the Rydberg-biased freezing regime where the system is described by a product state.

pure state. Whereas, for the second atom (subsystem B), $\mathrm{Tr}\,(\hat{\rho}_B^2)$ decreases and eventually converges to $1/2$ indicating that it is in a completely mixed state, i.e. a mixture of $|g\rangle$ and $|r\rangle$ with equal populations. As a consequence, the density matrix of the whole system is not completely mixed and $\mathrm{Tr}\,(\hat{\rho}_{AB}^2)$ converges to $1/2$. The dynamics of discord shown in figure 12(b) is as expected, in the initial period of time the correlations build up in the system due to large interactions, but exhibiting non-periodic oscillations, and eventually converge to a small value due to the Rydberg-biased freezing, as the system approaches steady state.

Note that we also obtained the analytical results for steady state density matrices, the purity of the system and subsystems, see appendix B, and are in excellent agreement with the exact numerical calculations. The comparison is made in figure 10.

7. Conclusions

In conclusion, we studied the dynamics and the quantum correlations in a minimal setup of two two-level Rydberg atoms driven continuously and independently by two distinct laser fields. In particular, we analyzed the effect of an offset in Rabi frequencies between the coupling fields on the Rydberg excitation dynamics, in the presence of Rydberg–Rydberg

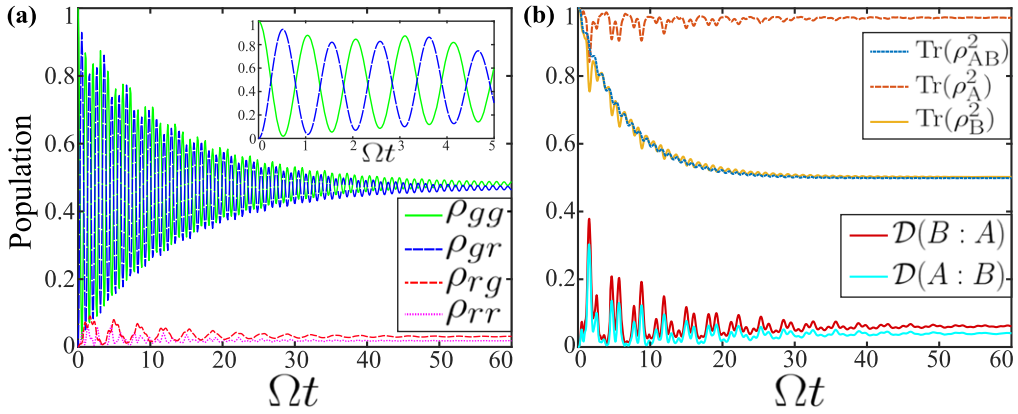

Figure 12. (a) The populations versus time for $\omega/\Omega = V_0/\Omega = 5$ and $\Gamma/\Omega = 0.1$. The inset shows the same for the initial period of time. (b) shows the time evolution of both the quantum discords, and the purity of the total system and subsystems, for the dynamics shown in (a).

interactions. Interestingly, we identified novel features in the system: amplifying the driving in one atom freezes the dynamics in the second atom, in the blockade regime. In addition to the Rydberg-biased freezing effect, a non-monotonous behaviour of doubly excited state population as a function interaction strength for small Rabi-offsets is observed. The effective Hamiltonians obtained via unitary transformations at various limits of system parameters provide us with analytical solutions for the dynamics. They are found to be in excellent agreement with the complete numerical calculations. The quantum discords for both the coherent and dissipative dynamics are studied. We also demonstrate that the quantum correlations can be controlled using a time-dependent Rabi-offset. Our studies open up a new possibility to engineer quantum states or correlations in a Rydberg atom setup or in any coupled two-level system. As an outlook, the immediate questions would be to extend the studies to more than two atoms, and also at different geometries.

Acknowledgments

We acknowledge the funding from the Indo-French Centre for the Promotion of Advanced Research, UKIERI-UGC Thematic Partnership No. IND/CONT/G/16-17/ 73 UKIERI-UGC project and UGC for UGC-CSIR NET-JRF/SRF.

Appendix A. Perturbation theory in the weak interaction limit

We write the Hamiltonian in equation (3) as $\hat{H} = \hat{H}_C + \hat{H}_V$ where $\hat{H}_C = (\Omega/2)\sum_{i=1}^{2}\hat{\sigma}_x^i + (\omega/2)\hat{\sigma}_x^2$ and $\hat{H}_V = V_0\hat{\sigma}_{rr}^1\hat{\sigma}_{rr}^2$. Treating $\hat{H}_V$ as a perturbation, we obtain the perturbative corrections to the eigenvectors and eigenvalues of $\hat{H}_C$ using non-degenerate perturbation theory, which demands that $\omega \neq 0$. The eigenvalues of the unperturbed Hamiltonian $\hat{H}_C$ and the eigenvectors in the basis $\{|gg\rangle, |gr\rangle, |rg\rangle, |rr\rangle\}$:

$$E_1^0 = \frac{-(2\Omega+\omega)}{2}, \qquad |\Psi_1^0\rangle = \frac{1}{2}\begin{bmatrix}1\\-1\\-1\\1\end{bmatrix} \tag{A.1}$$

$$E_2^0 = \frac{\omega}{2}, \qquad |\Psi_2^0\rangle = \frac{1}{2}\begin{bmatrix}-1\\-1\\1\\1\end{bmatrix} \tag{A.2}$$

$$E_3^0 = \frac{-\omega}{2}, \qquad |\Psi_3^0\rangle = \frac{1}{2}\begin{bmatrix}-1\\1\\-1\\1\end{bmatrix} \tag{A.3}$$

$$E_4^0 = \frac{2\Omega+\omega}{2}, \qquad |\Psi_4^0\rangle = \frac{1}{2}\begin{bmatrix}1\\1\\1\\1\end{bmatrix}. \tag{A.4}$$

The first-order correction to all the eigenvalues is simply $E_i^1 = \langle\Psi_i^0|\hat{H}_V|\Psi_i^0\rangle = V_0/4$, and we get the second-order corrections as:

$$E_1^2 = -V_0^2\left(\frac{(2\Omega+\omega)^2+\Omega(\Omega+\omega)}{16\Omega(\Omega+\omega)(2\Omega+\omega)}\right) = -E_4^2 \tag{A.5}$$

$$E_2^2 = -V_0^2\left(\frac{\omega^2-\Omega(\Omega+\omega)}{16\Omega\omega(\Omega+\omega)}\right) = -E_3^2. \tag{A.6}$$

The first-order correction to the eigenstates is obtained by

$$|\Psi_i^1\rangle = \sum_{j\neq i}\frac{\langle\Psi_j^0|H_V|\Psi_i^0\rangle}{E_i^0-E_j^0}|\Psi_j^0\rangle, \tag{A.7}$$

which then gives us

$$|\Psi_1^1\rangle = \frac{-V_0/8}{(\Omega+\omega)}\begin{bmatrix}-1\\-1\\1\\1\end{bmatrix} - \frac{V_0/8}{\Omega}\begin{bmatrix}-1\\1\\-1\\1\end{bmatrix} - \frac{V_0/8}{(2\Omega+\omega)}\begin{bmatrix}1\\1\\1\\1\end{bmatrix}. \tag{A.8}$$

Thus, we have up to the first-order correction in V_0, the first eigenvector:

$$|\Psi_1\rangle = |\Psi_1^0\rangle + |\Psi_1^1\rangle = \frac{1}{2}\begin{bmatrix} \frac{1}{4}\left(\frac{V_0}{\Omega+\omega} + \frac{V_0}{\Omega} - \frac{V_0}{2\Omega+\omega}\right) + 1 \\ \frac{1}{4}\left(\frac{V_0}{\Omega+\omega} - \frac{V_0}{\Omega} - \frac{V_0}{2\Omega+\omega}\right) - 1 \\ \frac{1}{4}\left(-\frac{V_0}{\Omega+\omega} + \frac{V_0}{\Omega} - \frac{V_0}{2\Omega+\omega}\right) - 1 \\ -\frac{1}{4}\left(\frac{V_0}{\Omega+\omega} + \frac{V_0}{\Omega} + \frac{V_0}{2\Omega+\omega}\right) + 1 \end{bmatrix}. \tag{A.9}$$

Similarly, the remaining eigenvectors are obtained as

$$|\Psi_2\rangle = |\Psi_2^0\rangle + |\Psi_2^1\rangle = \frac{1}{2}\begin{bmatrix} \frac{1}{4}\left(\frac{V_0}{\Omega+\omega} - \frac{V_0}{\omega} - \frac{V_0}{\Omega}\right) - 1 \\ \frac{1}{4}\left(-\frac{V_0}{\Omega+\omega} + \frac{V_0}{\omega} - \frac{V_0}{\Omega}\right) - 1 \\ -\frac{1}{4}\left(\frac{V_0}{\Omega+\omega} + \frac{V_0}{\omega} + \frac{V_0}{\Omega}\right) + 1 \\ \frac{1}{4}\left(\frac{V_0}{\Omega+\omega} + \frac{V_0}{\omega} - \frac{V_0}{\Omega}\right) + 1 \end{bmatrix} \tag{A.10}$$

$$|\Psi_3\rangle = |\Psi_3^0\rangle + |\Psi_3^1\rangle = \frac{1}{2}\begin{bmatrix} \frac{1}{4}\left(\frac{V_0}{\Omega} + \frac{V_0}{\omega} - \frac{V_0}{\Omega+\omega}\right) - 1 \\ -\frac{1}{4}\left(\frac{V_0}{\Omega} - \frac{V_0}{\omega} + \frac{V_0}{\Omega+\omega}\right) + 1 \\ -\frac{1}{4}\left(\frac{V_0}{\Omega} + \frac{V_0}{\omega} + \frac{V_0}{\Omega+\omega}\right) - 1 \\ \frac{1}{4}\left(\frac{V_0}{\Omega} - \frac{V_0}{\omega} - \frac{V_0}{\Omega+\omega}\right) + 1 \end{bmatrix} \tag{A.11}$$

$$|\Psi_4\rangle = |\Psi_4^0\rangle + |\Psi_4^1\rangle = \frac{1}{2}\begin{bmatrix} \frac{1}{4}\left(\frac{V_0}{2\Omega+\omega} - \frac{V_0}{\Omega} - \frac{V_0}{\Omega+\omega}\right) + 1 \\ \frac{1}{4}\left(-\frac{V_0}{2\Omega+\omega} - \frac{V_0}{\Omega} + \frac{V_0}{\Omega+\omega}\right) + 1 \\ \frac{1}{4}\left(-\frac{V_0}{2\Omega+\omega} + \frac{V_0}{\Omega} - \frac{V_0}{\Omega+\omega}\right) + 1 \\ \frac{1}{4}\left(\frac{V_0}{2\Omega+\omega} + \frac{V_0}{\Omega} + \frac{V_0}{\Omega+\omega}\right) + 1 \end{bmatrix}. \tag{A.12}$$

Then, writing the general time-dependent solution as:

$$\begin{aligned} |\Psi(t)\rangle = {} & Ae^{-iE_1 t}|\Psi_1\rangle + Be^{-iE_2 t}|\Psi_2\rangle \\ & + Ce^{-iE_3 t}|\Psi_3\rangle + De^{-iE_4 t}|\Psi_4\rangle, \end{aligned} \tag{A.13}$$

with $E_i = E_i^0 + E_i^1 + E_i^2$ and $|\Psi(t=0)\rangle = |gg\rangle$. Using the initial condition and solving a set of coupled linear equations we get the expressions for the co-efficients:

$$\begin{aligned} A = {} & \frac{2\Omega(\Omega+\omega)(2\Omega+\omega)}{\Lambda}[64\omega^2\Omega^3(\Omega+\omega)^3(2\Omega+\omega) \\ & + 16V_0\omega^2\Omega^2(\Omega+\omega)^2 \\ & \times (\omega^2 + 3\omega\Omega + 3\Omega^2) + 4V_0^2\Omega(\Omega+\omega)(2\Omega+\omega) \\ & \times (\omega^4 + 4\omega^3\Omega + 5\omega^2\Omega^2 + 2\omega\Omega^3 + \Omega^4) \\ & + V_0^3(\Omega^6 - 3\Omega^5(\Omega+\omega) + 3\Omega^3(\Omega+\omega)^3 \\ & - 3\Omega(\Omega+\omega)^5 + (\Omega+\omega)^6)] \end{aligned}$$

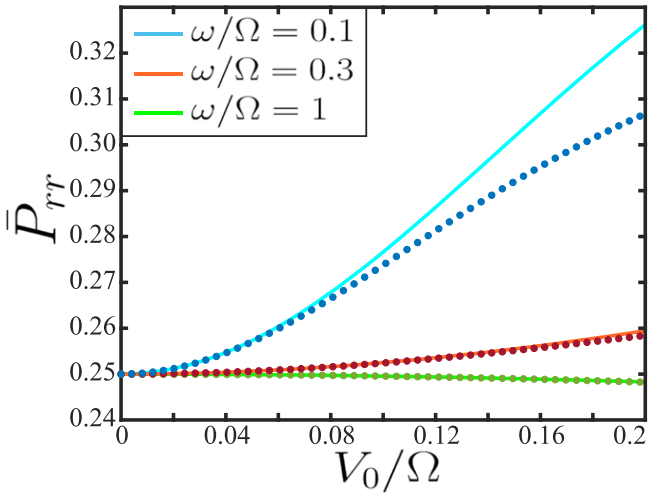

Figure A1. The time average population in $|rr\rangle$ state obtained using the perturbation theory (solid lines) in the weak interaction limit and the exact numerical solution (dotted lines) as a function of V_0 for different ω. The initial increment of $\bar{P}_{rr}$ in V_0/Ω for small ω/Ω, discussed in section 3, is well captured by the second-order perturbation theory.

$$\begin{aligned} B = {} & \frac{-2\Omega\omega(\Omega+\omega)}{\Lambda}[64\omega\Omega^3(\Omega+\omega)^3(2\Omega+\omega)^2 \\ & + 16V_0\Omega^2(\Omega+\omega)^2(2\Omega+\omega)^2 \\ & \times (\omega^2 + \omega\Omega + \Omega^2) + 4V_0^2\omega\Omega(\Omega+\omega) \\ & \times (\omega^4 + 4\omega^3\Omega + 5\omega^2\Omega^2 + 2\omega\Omega^3 + \Omega^4) \\ & + V_0^3(\Omega^6 + 3\Omega^5(\Omega+\omega) - 3\Omega^3(\Omega+\omega)^3 \\ & + 3\Omega(\Omega+\omega)^5 + (\Omega+\omega)^6)] \end{aligned}$$

$$\begin{aligned} C = {} & \frac{2\Omega\omega(\Omega+\omega)}{\Lambda}[-64\omega\Omega^3(\Omega+\omega)^3(2\Omega+\omega)^2 \\ & + 16V_0\Omega^2(\Omega+\omega)^2(2\Omega+\omega)^2 \\ & \times (\omega^2 + \omega\Omega + \Omega^2) - 4V_0^2\omega\Omega(\Omega+\omega) \\ & \times (\omega^4 + 4\omega^3\Omega + 5\omega^2\Omega^2 + 2\omega\Omega^3 + \Omega^4) \\ & + V_0^3(\Omega^6 + 3\Omega^5(\Omega+\omega) - 3\Omega^3(\Omega+\omega)^3 \\ & + 3\Omega(\Omega+\omega)^5 + (\Omega+\omega)^6)] \end{aligned}$$

$$\begin{aligned} D = {} & \frac{2\Omega(\Omega+\omega)(2\Omega+\omega)}{\Lambda}[64\omega^2\Omega^3(\Omega+\omega)^3 \\ & \times (2\Omega+\omega) - 16V_0\omega^2\Omega^2(\Omega+\omega)^2 \\ & \times (\omega^2 + 3\omega\Omega + 3\Omega^2) + 4V_0^2\Omega(\Omega+\omega)(2\Omega+\omega) \\ & \times (\omega^4 + 4\omega^3\Omega + 5\omega^2\Omega^2 + 2\omega\Omega^3 + \Omega^4) \\ & + V_0^3(-\Omega^6 + 3\Omega^5(\Omega+\omega) - 3\Omega^3(\Omega+\omega)^3 \\ & + 3\Omega(\Omega+\omega)^5 - (\Omega+\omega)^6)], \end{aligned}$$

where $\Lambda = 256\omega^2\Omega^4(\Omega+\omega)^4(2\Omega+\omega)^2 + 32V_0^2\Omega^2(\Omega+\omega)^2(\Omega^4 + (\Omega+\omega)^4) + \frac{V_0^4}{2}(\Omega^8 + (\Omega+\omega)^8 + \omega^4(2\Omega+\omega)^4)$. From above expressions it is straightforward to obtain $P_{rr}(t)$, and finally we have the time average population in the $|rr\rangle$ state as

$$\begin{aligned} \bar{P}_{rr} = {} & A^2 f_-^2(\omega,\Omega) + B^2 g_+^2(\omega,\Omega) \\ & + C^2 g_-^2(\omega,\Omega) + D^2 f_+^2(\omega,\Omega) \end{aligned} \tag{A.14}$$

where the functions

$$f_{\pm}(\omega, \Omega) = \frac{1}{2} \pm \frac{V_0}{8}\left[\frac{(2\Omega + \omega)^2 + \Omega(\Omega + \omega)}{\Omega(\Omega + \omega)(2\Omega + \omega)}\right] \quad \text{(A.15)}$$

$$g_{\pm}(\omega, \Omega) = \frac{1}{2} \pm \frac{V_0}{8}\left[\frac{\Omega(\Omega + \omega) - \omega^2}{\Omega\omega(\Omega + \omega)}\right]. \quad \text{(A.16)}$$

The perturbation theory results comparing that of exact numerical solutions are shown in figure A1.

Appendix B. Analytical results for the steady state density matrices and purity of the system and subsystems

On solving $\dot{\rho}(t) = 0$, the steady state density matrix of the system is obtained as:

$$\begin{aligned}\rho_{AB} = \frac{1}{\kappa}[&(V_0^2(\Gamma^2 + \Omega^2 + (\Omega + \omega)^2) \\ &+ (\Gamma^2 + \Omega^2)(\Gamma^2 + (\Omega + \omega)^2))|gg\rangle\langle gg| \\ &+(V_0^2 + \Gamma^2 + \Omega^2)(\Omega + \omega)^2|gr\rangle\langle gr| + \Omega^2(V_0^2 + \Gamma^2 \\ &+(\Omega + \omega)^2)|rg\rangle\langle rg| + \Omega^2(\Omega + \omega)^2|rr\rangle\langle rr| \\ &+\Omega(V_0^2 + \Gamma^2)(\Omega + \omega)(|gr\rangle\langle rg| + \text{H.c.}) \\ &+((\Omega + \omega)(i\Gamma - V_0)(\Gamma^2 + \Omega^2 - iV_0\Gamma)|gg\rangle\langle gr| + \text{H.c.}) \\ &+(\Omega(-V_0 + i\Gamma)(\Gamma^2 + (\Omega + \omega)^2 - iV_0\Gamma)|gg\rangle\langle rg| + \text{H.c.}) \\ &+(-\Gamma(iV_0 + \Gamma)\Omega(\Omega + \omega)|gg\rangle\langle rr| + \text{H.c.}) \\ &+((-V_0 + i\Gamma)\Omega(\Omega + \omega)^2|gr\rangle\langle rr| + \text{H.c.}) \\ &+((iV_0 + \Gamma)\Omega^2(\Omega + \omega)|rg\rangle\langle rr| + \text{H.c.})],\end{aligned} \quad \text{(B.1)}$$

and that of subsystems are

$$\begin{aligned}\rho_A = \frac{1}{\kappa}[&(V_0^2(\Gamma^2 + 2\omega^2 + 4\omega\Omega + 3\Omega^2) \\ &+ (\Gamma^2 + \Omega^2)(\Gamma^2 + 2(\Omega + \omega)^2))|g\rangle\langle g| \\ &+ \Omega^2(V_0^2 + \Gamma^2 + 2(\Omega + \omega)^2)|r\rangle\langle r| + (\Omega(iV_0^2\Gamma \\ &- 2V_0(\Omega + \omega)^2 + i\Gamma(\Gamma^2 + 2(\Omega + \omega)^2))|g\rangle\langle r| + \text{H.c.})]\end{aligned}$$

$$\begin{aligned}\rho_B = \frac{1}{\kappa}[&(V_0^2(\Gamma^2 + \omega^2 + 2\omega\Omega + 3\Omega^2) \\ &+ (\Gamma^2 + 2\Omega^2)(\Gamma^2 + (\Omega + \omega)^2))|g\rangle\langle g| \\ &+ (\Omega + \omega)^2(V_0^2 + \Gamma^2 + 2\Omega^2)|r\rangle\langle r| - ((\Omega + \omega)(V_0 - i\Gamma) \\ &\times (\Gamma^2 + 2\Omega^2 - iV_0\Gamma)|g\rangle\langle r| + \text{H.c.})]\end{aligned}$$

where

$$\begin{aligned}\kappa = &V_0^2(\Gamma^2 + 2\omega^2 + 4\Omega\omega + 4\Omega^2) \\ &+ (\Gamma^2 + 2\Omega^2)(\Gamma^2 + 2(\Omega + \omega)^2).\end{aligned} \quad \text{(B.2)}$$

The purity of the system and subsystems are obtained as:

$$\begin{aligned}\text{Tr}(\rho_{AB}^2) = \frac{1}{\kappa^2}[&(\Gamma^4 + 4\Gamma^2\Omega^2 + 2\Omega^4) \\ &\times (\Gamma^4 + 4\Gamma^2(\Omega + \omega)^2 + 2(\Omega + \omega)^4) \\ &+ V_0^4(\Gamma^4 + 4\Gamma^2(2\Omega^2 + 2\Omega\omega + \omega^2) + 2(2\Omega^2 \\ &+ 2\Omega\omega + \omega^2)^2) \\ &+ V_0^2(\Gamma^6 + 4\Gamma^4(2\Omega^2 + 2\Omega\omega + \omega^2) \\ &+ 4\Omega^2(\Omega + \omega)^2(2\Omega^2 + 2\Omega\omega + \omega^2) \\ &+ 2\Gamma^2(\omega^4 + 4\omega^3\Omega + 11\omega^2\Omega^2 + 14\omega\Omega^3 + 7\Omega^4))]\end{aligned}$$

$$\begin{aligned}\text{Tr}(\rho_A^2) = \frac{1}{\kappa^2}[&\Omega^4(V_0^2 + \Gamma^2 + 2(\Omega + \omega)^2)^2 \\ &+ 2(V_0^2 + \Gamma^2)\Omega^2((\Gamma^2 + 2(\Omega + \omega)^2)^2 + V_0^2\Gamma^2) \\ &+ (\Gamma^4 + 2\Omega^2(\Omega + \omega)^2 + V_0^2(\Gamma^2 + 2\omega^2 + 3\Omega^2) \\ &+ 4\Omega\omega V_0^2 + \Gamma^2(2\omega^2 + 3\Omega^2 + 4\Omega\omega))^2]\end{aligned}$$

$$\begin{aligned}\text{Tr}(\rho_B^2) = \frac{1}{\kappa^2}[&(\Omega + \omega)^4(V_0^2 + \Gamma^2 + 2\Omega^2)^2 \\ &+ 2(V_0^2 + \Gamma^2)(\Omega + \omega)^2((\Gamma^2 + 2\Omega^2)^2 + V_0^2\Gamma^2) \\ &+ (\Gamma^4 + 2\Omega^2(\Omega + \omega)^2 + V_0^2(\Gamma^2 + \omega^2 + 3\Omega^2) \\ &+ 2\Omega\omega V_0^2 + \Gamma^2(\omega^2 + 3\Omega^2 + 2\Omega\omega))^2].\end{aligned}$$

For $\omega = 0$, the expressions for purity become

$$\begin{aligned}\text{Tr}(\rho_A^2) = \text{Tr}(\rho_B^2) = \frac{1}{\kappa^2}[&V_0^4(\Gamma^4 + 8\Gamma^2\Omega^2 + 10\Omega^4) \\ &+ V_0^2(2\Gamma^6 + 16\Gamma^4\Omega^2 + 32\Gamma^2\Omega^4 + 24\Omega^6) \\ &+ \Gamma^8 + 8\Gamma^6\Omega^2 + 22\Gamma^4\Omega^4 + 24\Gamma^2\Omega^6 + 8\Omega^8]\end{aligned} \quad \text{(B.3)}$$

$$\begin{aligned}\text{Tr}(\rho_{AB}^2) = \frac{1}{\kappa^2}[&(\Gamma^4 + 4\Gamma^2\Omega^2 + 2\Omega^4)^2 + V_0^4(\Gamma^4 + 8\Gamma^2\Omega^2 + 8\Omega^4) \\ &+ 2V_0^2(\Gamma^6 + 8\Gamma^4\Omega^2 + 14\Gamma^2\Omega^4 + 8\Omega^6)],\end{aligned} \quad \text{(B.4)}$$

and for $\omega = 0$, the parameter κ reduces to,

$$\kappa = V_0^2(\Gamma^2 + 4\Omega^2) + (\Gamma^2 + 2\Omega^2)^2. \quad \text{(B.5)}$$

ORCID iDs

Vineesha Srivastava https://orcid.org/0000-0002-8382-5096
Ankita Niranjan https://orcid.org/0000-0003-3095-4094

References

[1] Saffman M, Walker T G and Mølmer K 2010 *Rev. Mod. Phys.* **82** 2313
[2] Löw R, Weimer H, Nipper J, Balewski J B, Butscher B, Büchler H P and Pfau T 2012 *J. Phys. B: At. Mol. Opt. Phys.* **45** 113001
[3] Browaeys A, Barredo D and Lahaye T 2016 *J. Phys. B: At. Mol. Opt. Phys.* **49** 152001
[4] Jones M P A, Marcassa L G and Shaffer J P 2017 *J. Phys. B: At. Mol. Opt. Phys.* **50** 060202

[5] Béguin L, Vernier A, Chicireanu R, Lahaye T and Browaeys A 2013 *Phys. Rev. Lett.* **110** 263201
[6] Lukin M D, Fleischhauer M, Cote R, Duan L M, Jaksch D, Cirac J I and Zoller P 2001 *Phys. Rev. Lett.* **87** 037901
[7] Gaëtan A, Miroshnychenko Y, Wilk T, Chotia A, Viteau M, Comparat D, Pillet P, Browaeys A and Grangier P 2009 *Nat. Phys.* **5** 115
[8] Urban E, Johnson T A, Henage T, Isenhower L, Yavuz D D, Walker T G and Saffman M 2009 *Nat. Phys.* **5** 110
[9] Weimer H, Müller M, Lesanovsky I, Zoller P and Büchler H P 2010 *Nat. Phys.* **6** 382
[10] Schauß P, Cheneau M, Endres M, Fukuhara T, Hild S, Omran A, Pohl T, Gross C, Kuhr S and Bloch I 2012 *Nature* **491** 87
[11] Barredo D, Labuhn H, Ravets S, Lahaye T, Browaeys A and Adams C S 2015 *Phys. Rev. Lett.* **114** 113002
[12] Schauß P, Zeiher J, Fukuhara T, Hild S, Cheneau M, Macrì T, Pohl T, Bloch I and Groß C 2015 *Science* **347** 1455
[13] Zeiher J, Van Bijnen R, Schauß P, Hild S, Choi J Y, Pohl T, Bloch I and Gross C 2016 *Nat. Phys.* **12** 1095
[14] Bernien H *et al* 2017 *Nature* **551** 579
[15] Zeiher J, Choi J Y, Rubio-Abadal A, Pohl T, van Bijnen R, Bloch I and Gross C 2017 *Phys. Rev.* X **7** 041063
[16] Marcuzzi M, Minář J C V, Barredo D, de Léséleuc S, Labuhn H, Lahaye T, Browaeys A, Levi E and Lesanovsky I 2017 *Phys. Rev. Lett.* **118** 063606
[17] Gross C and Bloch I 2017 *Science* **357** 995
[18] Jaksch D, Cirac J I, Zoller P, Rolston S L, Côté R and Lukin M D 2000 *Phys. Rev. Lett.* **85** 2208
[19] Wilk T, Gaëtan A, Evellin C, Wolters J, Miroshnychenko Y, Grangier P and Browaeys A 2010 *Phys. Rev. Lett.* **104** 010502
[20] Isenhower L, Urban E, Zhang X L, Gill A T, Henage T, Johnson T A, Walker T G and Saffman M 2010 *Phys. Rev. Lett.* **104** 010503
[21] Saffman M 2016 *J. Phys. B: At. Mol. Opt. Phys.* **49** 202001
[22] Ryabtsev I I, Tretyakov D B, Beterov I I and Entin V M 2010 *Phys. Rev. Lett.* **104** 073003
[23] Ravets S, Labuhn H, Barredo D, Béguin L, Lahaye T and Browaeys A 2014 *Nat. Phys.* **10** 914
[24] Labuhn H, Ravets S, Barredo D, Béguin L, Nogrette F, Lahaye T and Browaeys A 2014 *Phys. Rev.* A **90** 023415
[25] Ravets S, Labuhn H, Barredo D, Lahaye T and Browaeys A 2015 *Phys. Rev.* A **92** 020701
[26] Jau Y Y, Hankin A M, Keating T, Deutsch I H and Biedermann G W 2016 *Nat. Phys.* **12** 71
[27] de Léséleuc S, Barredo D, Lienhard V, Browaeys A and Lahaye T 2017 *Phys. Rev. Lett.* **119** 053202
[28] Zeng Y, Xu P, He X, Liu Y, Liu M, Wang J, Papoular D J, Shlyapnikov G V and Zhan M 2017 *Phys. Rev. Lett.* **119** 160502
[29] Picken C J, Legaie R, McDonnell K and Pritchard J D 2018 *Quantum Science and Technology* **4** 015011
[30] Levine H, Keesling A, Omran A, Bernien H, Schwartz S, Zibrov A S, Endres M, Greiner M, Vuletić V and Lukin M D 2018 *Phys. Rev. Lett.* **121** 123603
[31] Ott H 2016 *Rep. Prog. Phys.* **79** 054401
[32] Kuhr S 2016 *Natl Sci. Rev.* **3** 170
[33] De Léséleuc S, Barredo D, Lienhard V, Browaeys A and Lahaye T 2018 *Phys. Rev.* A **97** 053803
[34] Li W, Glaetzle A W, Nath R and Lesanovsky I 2013 *Phys. Rev.* A **87** 052304
[35] Nath R, Dalmonte M, Glaetzle A W, Zoller P, Schmidt-Kaler F and Gerritsma R 2015 *New J. Phys.* **17** 065018
[36] Maller K, Lichtman M, Xia T, Sun Y, Piotrowicz M, Carr A, Isenhower L and Saffman M 2015 *Phys. Rev.* A **92** 022336
[37] Eisert J, Cramer M and Plenio M B 2010 *Rev. Mod. Phys.* **82** 277
[38] Modi K, Brodutch A, Cable H, Paterek T and Vedral V 2012 *Rev. Mod. Phys.* **84** 1655
[39] Amico L, Fazio L, Osterloh A and Vedral V 2008 *Rev. Mod. Phys.* **80** 517
[40] Dillenschneider R 2008 *Phys. Rev.* B **78** 224413
[41] Latorre J I and Riera A 2009 *J. Phys. A: Math. Theor.* **42** 504002
[42] Chen Y X and Li S W 2010 *Phys. Rev.* A **81** 032120
[43] Wang C, Zhang Y Y and Chen Q H 2012 *Phys. Rev.* A **85** 052112
[44] Bera A, Das T, Sadhukhan D, Roy S S, De A S and Sen U 2017 *Rep. Prog. Phys.* **81** 024001
[45] Levin M and Wen X-G 2006 *Phys. Rev. Lett.* **96** 110405
[46] Kitaev A and Preskill J 2006 *Phys. Rev. Lett.* **96** 110404
[47] Jiang H C, Wang Z and Balents L 2012 *Nat. Phys.* **8** 902
[48] Isakov S V, Hastings M B and Melko R G 2011 *Nat. Phys.* **7** 772
[49] Zhang Y, Grover T and Vishwanath A 2011 *Phys. Rev. Lett.* **107** 067202
[50] Bennett C H, DiVincenzo D P, Smolin J A and Wootters W K 1996 *Phys. Rev.* A **54** 3824
[51] Bennett C H, Bernstein H J, Popescu S and Schumacher B 1996 *Phys. Rev.* A **53** 2046
[52] Henderson L and Vedral V 2001 *J. Phys. A: Math. Gen.* **34** 6899
[53] Ollivier H and Zurek W H 2001 *Phys. Rev. Lett.* **88** 017901
[54] Datta A, Shaji A and Caves C M 2008 *Phys. Rev. Lett.* **100** 050502
[55] Lanyon B P, Barbieri M, Almeida M P and White A G 2008 *Phys. Rev. Lett.* **101** 200501
[56] Okrasa M and Walczak Z 2011 *EPL (Europhysics Letters)* **96** 60003
[57] Islam R, Ma R, Preiss P M, Tai M E, Lukin A, Rispoli M and Greiner M 2015 *Nature* **528** 77
[58] Kaufman A M, Tai M E, Lukin A, Rispoli M, Schittko R, Preiss P M and Greiner M 2016 *Science* **353** 794
[59] Hu A, Lee T E and Clark1 C W 2013 *Phys. Rev.* A **88** 053627
[60] Fan C H, Yan D, Liu Y M and Wu J H 2017 *J. Phys. B: At. Mol. Opt. Phys.* **50** 115501
[61] Mourachko I, Comparat D, de Tomasi F, Fioretti A, Nosbaum P, Akulin V M and Pillet P 1998 *Phys. Rev. Lett.* **80** 253
[62] Anderson W R, Veale J R and Gallagher T F 1998 *Phys. Rev. Lett.* **80** 249
[63] Adesso G and Datta A 2010 *Phys. Rev. Lett.* **105** 030501
[64] Vedral V, Plenio M B, Rippin M A and Knight P L 1997 *Phys. Rev. Lett.* **78** 2275
[65] Vedral V and Plenio M B 1998 *Phys. Rev.* A **57** 1619
[66] Ates C, Pohl T, Pattard T and Rost J M 2007 *Phys. Rev. Lett.* **98** 023002
[67] Basak S, Chougale Y and Nath R 2018 *Phys. Rev. Lett.* **120** 123204
[68] Chougale Y and Nath R 2016 *J. Phys. B: At. Mol. Opt. Phys.* **49** 144005